Title
THE STRUCTURE OF SOLID SURFACES

Authors
Somorjai, G.A.
Kesmodel, L.L.

Publication Date
1974-02-01

Submitted for Publication

LBL-3135
Preprint

THE STRUCTURE OF SOLID SURFACES

G. A. Somorjai and L. L. Kesmodel

February, 1974

Prepared for the U. S. Atomic Energy Commission
under Contract W-7405-ENG-48

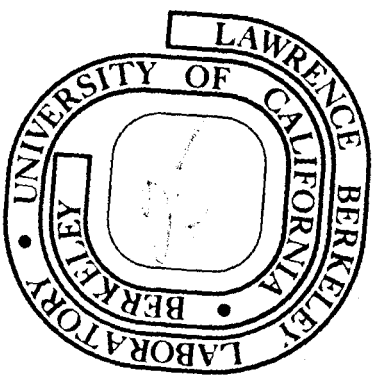

DISCLAIMER

THE STRUCTURE OF SOLID SURFACES

G. A. Somorjai and L. L. Kesmodel

Department of Chemistry, University of California

and Inorganic Materials Research Division, Lawrence Berkeley Laboratory

Berkeley, California -94720

February 1974

Submitted for publication as a chapter in the
MTP International Review of Science

TABLE OF CONTENTS

1. INTRODUCTION

The development of modern chemistry owes a great deal to techniques that permit the study of chemical phenomena on an atomic or molecular scale. Great advances in our understanding of the structure of molecules in the gas phase have come from the development of spectroscopy, from electron spectroscopy (ESCA) to microwave spectroscopy. These studies served as the basis for deciphering the molecular dynamics of gas phase reactions. In the solid state, x-ray, electron, and neutron diffraction studies of the atomic structure laid the foundation for the understanding of many solid state transport phenomena. In general, solving the structure, atomic or electronic, is the prerequisite to the unraveling of the chemical reaction dynamics.

In surface science the technique of low-energy electron diffraction (LEED) yields the structure of surfaces on an atomic scale. During the past ten years this technique has been providing detailed information on the structure of solid surfaces and on the structure of adsorbates. In the past five years an understanding of the nature of the diffraction of low-energy electrons has been achieved. That is, a theory has been developed that enables computation of the diffraction beam properties (intensity vs. energy) if the positions of the surface atoms are specified. Thus, surface crystallography has emerged as a new field of surface science that permits the determination of the unique positions of atoms on the surface from the intensities of the diffraction beams.

From these studies a physical picture of the surface atomic structure is emerging. We know now that for clean surfaces atoms may occupy sites

that are different from those expected from the projection of the bulk (x-ray) unit cell. High Miller index surfaces have a unique stepped surface structure and atoms in steps exhibit exceptional reactivity. The chemical compositon of diatomic and polyatomic solids may be very different from the bulk stoichiometry. Moreover, adsorbed gases and vapors form ordered surface structures and may undergo order-disorder transformations under the proper conditions of temperature and pressure.

In this paper we shall review the present status of surface crystallography and much of our knowledge of the atomic structure of surfaces and of adsorbed molecules. The method of surface structure analysis will be presented, and then we shall discuss the structure of clean solid surfaces of low and high Miller index. Finally we shall discuss the structure of adsorbed molecules of small and large size relative to the interatomic distance in the substrate plane.

Determination of the unique atomic position of adsorbates, their distance from the underlying plane of atoms and their bond angle, yields the fundamental experimental data needed to unravel the surface chemical bond. The structures of adsorbed molecules reveal the nature of adhesion or lubrication on a molecular scale. Finally, the ordered adsorbate structures often play a rate controlling role and are intermediates in catalyzed surface chemical reactions.

2. SURFACE STRUCTURE ANALYSIS BY LOW-ENERGY ELECTRON DIFFRACTION

2.1 Surface Geometry and Diffraction Conditions

In this section some of the general features of the diffraction of low-energy electrons from crystal surfaces are discussed and a notation appropriate to the description of surface structures is reviewed. In subsequent sections a detailed discussion of low-energy electron diffraction theory and application are presented.

A typical low-energy electron diffraction experiment (Fig. 1) consists of a monoenergetic beam of electrons (10 eV $\lesssim$ E $\lesssim$ 500 eV) incident on one face of a single crystal. Roughly one-half of the electrons are backscattered, and the elastically scattered fraction is allowed to impinge on a fluorescent screen. If the crystal surface is well-ordered, a diffraction pattern (Fig. 2) consisting of bright, well-defined spots will be displayed on the screen. The sharpness and overall intensity of the spots is related to the degree of order on the surface. Although the surface may be irregular on a microscopic and submicroscopic scale (e.g., consisting of atomic terraces and ledges) the presence of sharp diffraction features indicates that the surface is ordered on an atomic scale, the atoms lying in planes parallel to the surface characterized by a two-dimensional lattice structure. The size of these ordered domains determines the quality of the diffraction pattern. Because of experimental limitations on the coherence width of the electron beam, ordered domains larger than approximately 500 Å in diameter are not detectable. However, if the ordered domains become significantly smaller than 500 Å, the diffraction spots broaden and become less intense.

The presence of sharp diffraction features in the low-energy electron diffraction patterns establishes that crystal surfaces are ordered on an atomic scale. In addition, the positions and symmetry of the diffraction spots can be used to determine the two-dimensional periodicity of the ordered arrangement of surface atoms. We can imagine for the moment that the surface structure will be rather like the termination of the bulk structure along a crystal plane (e.g., the (100) plane of a cubic crystal) although there may be a rearrangement or <u>reconstruction</u> of the surface atoms from the bulk structure. The presence of the surface destroys the bull translational periodicity in the direction normal to the presumed planar surface. The translational periodicity of the solid parallel to the surface is retained and will be one of the five two-dimensional Bravais lattices.[1] The atoms lie in planes parallel to the surface and a translation $\underset{\sim}{T}$ in the plane of the form

$$\underset{\sim}{T} = n_1\underset{\sim}{a} + n_2\underset{\sim}{b} \tag{1}$$

takes each atom to an equivalent site. Here n_1 and n_2 are integers, and $\underset{\sim}{a}$ and $\underset{\sim}{b}$ are the primitive translation vectors that define the surface unit cell. The periodicity of the solid in the direction parallel to the surface is responsible for the basic momentum conservation law of diffraction theory that

$$\underset{\sim}{k}'_{\parallel} = \underset{\sim}{k}_{\parallel} + \underset{\sim}{g} \tag{2}$$

where $\underset{\sim}{k}_{\parallel}$ and $\underset{\sim}{k}'_{\parallel}$ are respectively the components of the incident and outgoing wave vector of the scattered electron in the direction <u>parallel</u> to the surface. The discrete set of vectors $\underset{\sim}{g}$

comprise the surface reciprocal mesh so that together with energy conservation ($E(\underset{\sim}{k}') = E(\underset{\sim}{k})$) Eq.(2) defines the directions of the allowed diffraction beams appearing in the diffraction pattern. In analogy with the x-ray crystallography of the bulk,[2] the primitive vectors $\underset{\sim}{a}^*$ and $\underset{\sim}{b}^*$ of the surface reciprocal mesh are related to the direct space vectors $\underset{\sim}{a}$ and $\underset{\sim}{b}$ by the equations

$$\underset{\sim}{a}^* = \frac{\underset{\sim}{b} \times \underset{\sim}{z}}{(\underset{\sim}{a} \cdot \underset{\sim}{b} \times \underset{\sim}{z})} \tag{3a}$$

$$\underset{\sim}{b}^* = \frac{\underset{\sim}{z} \times \underset{\sim}{a}}{(\underset{\sim}{a} \cdot \underset{\sim}{b} \times \underset{\sim}{z})} \tag{3b}$$

where $\underset{\sim}{z}$ is the surface normal. The allowed diffraction beams $\underset{\sim}{g}$ are formally labelled by beam indices (hk) according to the equation

$$\underset{\sim}{g} = 2\pi(h\,\underset{\sim}{a}^* + k\,\underset{\sim}{b}^*) \quad . \tag{4}$$

It is evident from Eq.(2) that the diffraction pattern gives a representation of the surface reciprocal lattice, and indeed the vectors $\underset{\sim}{a}^*$ and $\underset{\sim}{b}^*$ may be determined from a measurement of the beam angles. Then by application of relations inverse to Eq.(3) one may solve for the vectors $\underset{\sim}{a}$ and $\underset{\sim}{b}$ that define the surface unit cell. Fig. 3, for example, illustrates the relation of the direct and reciprocal space vectors for the case of the hexagonal Bravais lattice.

The basic complication of surface structure analysis via low-energy electron diffraction comes from the fact that observation of the diffraction pattern geometry serves only to determine the size and shape of the two-dimensional unit cell which characterizes the translational periodicity parallel to the surface. Critical information relating to structural variations

in the direction normal to the surface must be extracted from an analysis of the intensity of the diffracted beams. Such an intensity analysis is in principle required, for example, to determine the packing sequence and interlayer spacings of the top few atomic layers of a single-crystal surface. These types of analyses constitute the fundamental motivation and application of low-energy electron diffraction theory and are reviewed in Section 2.2.

It is appropriate at this point to discuss notational conventions[1,3] for classifying surface structures. In the simplest case, the surface structure is given by the termination of the bulk structure along a given crystal plane. The surface unit mesh in such cases is briefly referred to as (1 x 1), indicating that the lattice vectors $\underset{\sim}{a}$ and $\underset{\sim}{b}$ in the surface region are identical to those of the underlying bulk substrate, (e.g., Pt(111) - (1 x 1)). In more general cases the surface structure will differ greatly from that of the bulk substrate. An interesting example is the deposition of layers of foreign atoms (adsorbate) on the substrate material. Such adsorbed overlayer structures will in general have a periodicity different from that of the substrate and may even cause reconstruction of the substrate atoms near the surface. Another case is the reconstruction of the surface region of a chemically clean material as occurs, for example, in silicon. It is clear that the structure of the first several outer atomic layers of a particular system may be quite complex. Surface scientists often refer to this surface and near-surface region as the "selvedge."[1] It is reasoned that the selvedge region extends only a relatively short distance into the surface before the space group

symmetry of the bulk substrate is regained. The problem of surface structure analysis thus involves determination of the structure of the selvedge region and its orientation with respect to the undistorted bulk substrate.

It is frequently the case that the surface structures have unit cells that are integral multiples of the substrate unit cell. For example, the notation W(211) - (2 x 2) - H is conveniently used to refer to the adsorption of hydrogen on a (211) face of tungsten characterized by each axis of the adsorbate unit cell being twice that of the substrate. Such concise notation may also be profitably employed in cases where the surface structure is rotated in a simple fashion with respect to the substrate. As shown in Fig. 4, the c(2 x 2) structure on a square lattice substrate (where the symbol c indicates a "centered" mesh) may equivalently be designated as $p(\sqrt{2} \times \sqrt{2})$ - R45°. The latter notation indicates that the primitive cell of the surface structure is rotated by 45° with respect to that of the substrate, and the sides of the surface mesh are in the ratio of $\sqrt{2}$ to those of the substrate.

The notational scheme outlined above is suitable for simple surface structures and is commonly used in the literature. However, a more general matrix notation[3,4] is appropriate for complex structures. We consider a substrate primitive cell with translation vectors $\underset{\sim}{a}$ and $\underset{\sim}{b}$ and an overlayer structure with corresponding vectors $\underset{\sim}{a}_s$ and $\underset{\sim}{b}_s$. Defining a set of cartesian unit vectors $\hat{x}$ and $\hat{y}$ we can construct matrices $\underset{\approx}{A}$ and $\underset{\approx}{A}_s$ such that

$$\begin{bmatrix} \underset{\sim}{a} \\ \underset{\sim}{b} \end{bmatrix} = \underset{\approx}{A} \begin{bmatrix} \hat{x} \\ \hat{y} \end{bmatrix} \tag{5a}$$

and

$$\begin{bmatrix} \underset{\sim}{a}_s \\ \\ \underset{\sim}{b}_s \end{bmatrix} = \underset{\sim}{A}_s \begin{bmatrix} \hat{x} \\ \\ \hat{y} \end{bmatrix} \tag{5b}$$

The relationship between the unit meshes is compactly described by the transformation matrix $\underset{\sim}{G}$ satisfying

$$\underset{\sim}{A}_s = \underset{\sim}{G}\,\underset{\sim}{A} \tag{6}$$

As discussed by Estrup and McRae,[3] the determinant G of the matrix $\underset{\sim}{G}$ may be used to define the possible relationships between the substrate and overlayer nets. The nets are designated as <u>simply related</u>, <u>rationally related</u>, or <u>irrationally related</u> according to whether G is respectively an integer, a rational number, or an irrational number. Furthermore, the composite system formed by the superposition of the two nets is respectively designated above as a <u>simple</u> structure, a <u>coincidence-site</u> structure, or an <u>incoherent</u> structure. The incoherent superposition is not in itself describable by a net. However, the superposed system of either the simple or coincidence site structure is itself characterized by a Bravais net, and in these cases the overlayer and substrate are said to be <u>in register</u>. Returning then to the notational example of the c(2 x 2) structure on a square lattice substrate we find that the transformation matrix $\underset{\sim}{G}$ is $\begin{pmatrix} 1 & 1 \\ -1 & 1 \end{pmatrix}$ and the nets are simply related. Thus, the notation Ni(100) -$\begin{pmatrix} 1 & 1 \\ -1 & 1 \end{pmatrix}$- S(1/2) could be used to denote the C(2 x 2) adsorption of one-half monolayer of sulfur on a (100) face of nickel.

2.2 Theory of Low-Energy Electron Diffraction from Crystalline Surfaces

In the previous section some of the general features of elastic low-energy electron diffraction were set forth and the notation of surface crystallography was discussed. It was shown how observation of intensity pattern geometry may be used to determine the periodicity of the surface structures in the direction parallel to the surface. However, a principal result of this discussion was the necessity of an intensity analysis for elucidation of the surface structure in the direction normal to the surface. A case of great current interest, for example, is the determination of the registry of a chemisorbed overlayer with respect to the bulk substrate by means of low-energy electron diffraction intensity analyses. The standard such analysis in elastic low-energy electron diffraction involves the variation in the intensity of a given diffraction beam (spot) as a function of the incident beam energy. Experimentally, the intensity data is normally taken in the energy range $20 \lesssim E \lesssim 300$ eV by means of a spot photometer or Faraday collector. It is in this energy range that the scattered electrons are most surface sensitive. Theoretical calculations employing models of the surface atomic geometry are then compared to the experimental intensity-energy (I-V) profiles. Surface crystallography is, in principle, carried out by finding the (presumably unique) surface structure which optimizes the agreement between theory and experiment over a significantly large range of diffraction conditions (i.e., energy range, number of diffracted beams, and incident beam angles). In practice, such a procedure is rather difficult because the theoretical calculations must provide an adequate description of the complex nature of the electron-solid interaction

in the energy range relevant to low energy electron diffraction. Nevertheless, important strides have been made in recent years in constructing a suitable "microscopic" low-energy electron diffraction theory which is accompanied by manageable computation times and computer storage requirements. In addition, intensity-averaging procedures and intensity transform techniques (so-called "data reduction" methods) have been proposed as possible alternatives to the microscopic-model calculations. In the remainder of this section we review the microscopic low-energy electron diffraction theory and outline the essential features of the presently more tentative data reduction methods. In Section 2.3 recent applications of intensity analysis to surface crystallography are examined.

2.2.1 Microscopic-model theory

The goal of microscopic low-energy electron diffraction theory is a quantum mechanical formulation of the electron-solid scattering process and, in particular, calculations of the I-V profiles in which the main "adjustable parameter" is the surface atomic geometry itself. There are two major features of the electron-solid interaction evidenced in the I-V profiles and in other scattering data that the theory must provide for: (i) in contrast to the case of x-ray scattering, the elastic scattering cross-sections[5,6] for low-energy electrons from atoms are large --- on the order of 10 $\AA^2$/atom, and (ii) the incident electrons interact strongly with the valence electrons in the solid resulting in a high probability of inelastic scattering[6,11] (e.g., plasmon, particle-hole, and ion-core excitations) within the first few atomic layers of the surface. Features (i) and (ii) taken together with the wave-like behavior of the electrons[8] make low-energy

electron diffraction a sensitive probe of the surface atomic structure. Feature (i), however, renders the use of the simple kinematical[6] (single-scattering) theory inadequate in low-energy electron diffraction and necessitates the use of multiple scattering or so-called "dynamical" theories. Feature (ii), on the other hand, means that electrons are removed from the elastic electron beam due to "inelastic-collision damping"[11] with a characteristic mean free path $\lambda_{ee} \sim 3\text{-}10$ Å. The inelastic-collision damping tends to reduce, though by no means eliminates, the effect of multiple scattering. The presence of multiple-scattering introduces "secondary" maxima in the I-V profiles in addition to the "Bragg" peaks (from the analogous integral-order peaks of x-ray diffraction) anticipated from kinematical theory. Moreover, the effect of inelastic scattering has been shown to limit the amount of secondary structure --- generally smoothing and broadening the diffraction peaks.

There have been a number of formulations of low-energy electron diffraction theory which take multiple scattering and inelastic scattering into account.[7-16] Here we shall briefly outline the theory originally proposed by Beeby.[10] The theory was subsequently modified to include inelastic-collision damping by Duke and Tucker[11] and the approximate effects of lattice vibrations by Duke and Laramore.[16] The theory has much in common with other treatments, of course, and its presentation serves to illustrate both the degree of sophistication and limitations of the current theories.

The incident electron is taken to be in a plane-wave state with energy E and wave vector $\underline{k}$. The elastically scattered electrons are observed with the energy E and wave vector $\underline{k}'$. Following Beeby's formulation the scattered intensity is given by

$$I(\underset{\sim}{k} \to \underset{\sim}{k}') \propto \left| \int \exp(-i\underset{\sim}{k}' \cdot \underset{\sim}{r}') T(\underset{\sim}{r}', \underset{\sim}{r}) \exp(i\underset{\sim}{k} \cdot \underset{\sim}{r}) \, d\underset{\sim}{r} \, d\underset{\sim}{r}' \right|^2 \tag{7}$$

where T is the total scattering matrix satisfying

$$T(\underset{\sim}{r}', \underset{\sim}{r}) = V(\underset{\sim}{r}') \, \delta(\underset{\sim}{r} - \underset{\sim}{r}') + \int V(\underset{\sim}{r}') G_0(\underset{\sim}{r}' - \underset{\sim}{r}'') T(\underset{\sim}{r}'', \underset{\sim}{r}) \, d\underset{\sim}{r}'' \tag{8}$$

and $G_0(\underset{\sim}{r})$ is the usual outgoing free-particle propagator[17]

$$G_0(\underset{\sim}{r}) = \frac{1}{8\pi^3} \int \frac{\exp(i\underset{\sim}{k} \cdot \underset{\sim}{r}) d\underset{\sim}{k}}{E - \frac{\hbar^2 k^2}{2m} + i\varepsilon} \tag{9}$$

The crystal potential $V(\underset{\sim}{r})$ is taken to be a superposition of nonoverlapping ion-core potentials situated at lattice sites $\underset{\sim}{R}$:

$$V(\underset{\sim}{r}) = \sum_{\underset{\sim}{R}} v_{\underset{\sim}{R}}(\underset{\sim}{r} - \underset{\sim}{R}) \tag{10}$$

where $v_{\underset{\sim}{R}}(\underset{\sim}{r})$ is the ion-core potential at position $\underset{\sim}{R}$. Using Eqs. (8) and (10) it can be shown that[18]

$$\begin{aligned} T(\underset{\sim}{r}', \underset{\sim}{r}) = & \sum_{\underset{\sim}{R}} t_{\underset{\sim}{R}}(\underset{\sim}{r}' - \underset{\sim}{R}, \underset{\sim}{r} - \underset{\sim}{R}) \\ & + \sum_{\underset{\sim}{R} \neq \underset{\sim}{R}'} \int t_{\underset{\sim}{R}'}(\underset{\sim}{r}' - \underset{\sim}{R}', \underset{\sim}{r}'' - \underset{\sim}{R}) \, G_0(\underset{\sim}{r}''' - \underset{\sim}{r}''') \, t_{\underset{\sim}{R}}(\underset{\sim}{r}''' - \underset{\sim}{R}, \underset{\sim}{r} - \underset{\sim}{R}) \, d\underset{\sim}{r}'' \, d\underset{\sim}{r}''' \\ & + \ \ldots \end{aligned} \tag{11}$$

where the multiple scattering from the atom at $\underset{\sim}{R}$ is given by the single-site t-matrix

$$t_{\underset{\sim}{R}}(\underset{\sim}{r}', \underset{\sim}{r}) = v_{\underset{\sim}{R}}(\underset{\sim}{r}') \, \delta(\underset{\sim}{r} - \underset{\sim}{r}') + \int v_{\underset{\sim}{R}}(\underset{\sim}{r}') G_0(\underset{\sim}{r}' - \underset{\sim}{r}'') t_{\underset{\sim}{R}}(\underset{\sim}{r}'', \underset{\sim}{r}) \, d\underset{\sim}{r}'' \ . \tag{12}$$

Equation (11) is a useful result because it expresses the total scattering matrix in terms of successively higher order scatterings between single atomic sites with the important provision that no two successive scatterings

be off the same atom. It also allows for a precise treatment of the scattering from a single atom in terms of the t-matrix $\underset{\sim}{t}_R(\underset{\sim}{r},\underset{\sim}{r}')$ defined in Eq. (12). This is a non-trivial point, in view of the general inadequacy of Born approximation treatments of low-energy electron scattering from atomic potentials.

The reduction of Eq. (11) to an algebraic form and the performance of the sums over scattering paths is accomplished by a series of manipulations prescribed by Beeby. The reader is referred to the original papers[10,19] for details of the methods, but we mention here the essential points. The atomic potentials are assumed to be spherically symmetric so that the single-site t-matrices are appropriately expanded in an angular momentum representation. Each scattering is on the energy shell and may be defined in terms of the phase shifts[17]. Taking the atoms to lie in planes parallel to the surface, the planes are further divided into "subplanes" all of which have an identical structure termed the "substructure". The substructure is essentially the smallest structure common to the primitive cells of all the atomic planes parallel to the surface. Furthermore, each subplane, by construction, contains only one type of atom and thereby has scattering properties described by a single t-matrix. The subplane concept greatly facilitates the performance of the sums over scattering paths and naturally leads to the conceptual separation of scattering events taking place solely within subplanes and those linking subplanes. The final result for the scattered intensity is[10]

$$I(\underset{\sim}{k} \to \underset{\sim}{k}') \propto \left| \sum_{LL'} Y_L(\underset{\sim}{k}') Y_{L'}(\underset{\sim}{k}) \left[\sum_{\nu} \exp\left\{ i(\underset{\sim}{k} - \underset{\sim}{k}') \cdot \underset{\sim}{d}_{\nu} \right\} \underset{\sim}{T}_{\nu\nu} \right]_{LL'} \times \frac{(2\pi)^2}{A} \sum_{\underset{\sim}{g}} \delta(\underset{\sim}{k}_{\parallel} - \underset{\sim}{k}'_{\parallel} + \underset{\sim}{g}) \right|^2 \qquad (13)$$

where the index $\underline{L}$ denotes the pair of indices (ℓ,m), the $Y_L(\underset{\sim}{k})$ are the (real) spherical harmonics, and $\underline{A}$ is the area of the surface unit cell. The sum over delta functions expresses the conservation law of Eq. (4) arising from the two-dimensional periodicity of the subplanes. The variable $\underline{\nu}$ indexes a given subplane with its (fixed) origin centered on an atom at $\underset{\sim}{d}_\nu$. The matrix $\underset{\sim}{T}_{\nu}$ is defined by the equations

$$\underset{\sim}{T}_{\nu\nu} = \underset{\sim}{t}_{\nu} + \underset{\sim}{t}_{\nu} \sum_{\nu' (\neq \nu)} \underset{\sim}{G}^{\nu\nu'}(\underset{\sim}{k}) \underset{\sim}{T}_{\nu'\nu} \tag{14a}$$

$$\underset{\sim}{t}_{\nu\nu} = \underset{\sim}{t}_{\nu}(\kappa) \left\{ \underset{\sim}{1} - \underset{\sim}{G}^{SP}(\underset{\sim}{k}) \underset{\sim}{t}_{\nu}(\kappa) \right\}^{-1} \tag{14b}$$

where $\kappa^2 = 2mE/\hbar^2$. The matrices $\underset{\sim}{G}^{\nu\nu'}$ and $\underset{\sim}{G}^{SP}$ are appropriately defined structure factors similar to those found in the Korringa-Kohn-Rostoker method of energy band theory and are relatively straightforward to calculate. The matrix $\underset{\sim}{t}_{\nu}(\kappa)$ is a diagonal matrix for single-site scattering with elements

$$t_{\ell,\nu}(\kappa) = -\left(\frac{\hbar^2}{2m}\right) \left[\frac{\exp(2i\,\delta_\ell(\kappa)) - 1}{2i\kappa} \right] \tag{15}$$

where $\delta_\ell(\kappa)$ are the phase shifts evaluated for the type of scatterer in subplane $\underline{\nu}$. The matrix $\underset{\sim}{t}_{\nu}$ represents all of the scattering events taking place solely within the subplane $\underline{\nu}$. Finally, the matrix $\underset{\sim}{T}_{\nu}$ represents all of the scattering events which end in plane $\underline{\nu}$.

Although Eqs. (13) and (14) are not particularly transparent from a physical point-of-view, they do provide a straightforward mathematical procedure for calculating the intensities. Choosing $\underline{\ell}$ phase shifts to describe the electron-ion-core scattering and dividing the model structure into $\underline{N}$ subplanes essentially requires the inversion of an $(N\ell^2 \times N\ell^2)$ complex

matrix for exact solutions to Eq.(14a). As an example of the total computation time involved for such "exact" intensity calculations, Tong and Kesmodel[20] reported results with a computer program requiring approximately 30 seconds per energy point on a CDC 6600 machine and 6 seconds per point on a CDC 7600 machine for a model calculation utilizing 5 phase shifts and 5 atomic layers. The computer time and storage requirements rise rapidly as the number of layers or phase shifts needed for reasonable accuracy are increased. This fact has led to the proposal of various perturbation approaches to the solution of Eqs. (14) or similar equations.[21-24]

Duke and co-workers[11,16] modified Beeby's results to include an approximate treatment of inelastic-collision damping and the effects of lattice vibrations although the structure of the equations is unchanged. Briefly, the damping effects are introduced through the inclusion of an electronic self-energy term $\Sigma(\underset{\sim}{k},E)$ in the propagator of Eq. (9) and a boundary condition on the incident electron wave vector inside the solid which makes it a complex number. Physically, these prescriptions cause the electron wave fields inside the solid to be exponentially decaying, thereby reducing the effects of multiple scattering. The effects of lattice vibrations are included by means of a renormalization of the single-site t-matrices. In essence, the scattering at each site is modified by a Debye-Waller factor that accounts for the loss of electrons by quasielastic phonon scattering. The phonon scattering is termed quasielastic because the energy changes involved are very small ($\Delta E = \hbar\omega \approx 0.01$ eV), and the phonon-

scattered electrons are not separated from the purely elastic component in conventional low energy electron diffraction experiments. The phonon scattering, however, can change the momentum of the electrons significantly thereby causing a fraction of the electrons to be scattered (thermal diffuse scattering) into the background between the diffraction spots. The Debye-Waller corrections to the I-V profiles have the general effect of reducing the heights of the higher energy peaks in relation to those at lower energies, but such corrections may also change peak shapes significantly.

For computational reasons a number of simplifying assumptions are inevitably made. The atomic potentials are in principle obtained from self-consistent calculations appropriate to the surface region, but in practice bulk band structure potentials or potentials obtained from the overlap of atomic charge densities are employed. The effects of inelastic damping are normally included by a suitably parameterized electron self-energy term or by an optical potential model. Finally, the lattice vibrational amplitudes are taken to be spherically symmetric and for most calculations independent of distance from the surface. Several systematic calculations, primarily for clean metal surfaces, have indicated that the above approximations are acceptable for achieving adequate agreement with experimental I-V profiles taken at constant temperature. Obtaining the observed temperature dependence of the intensities requires more accurate treatments of the lattice vibrations.

2.2.2 Data reduction methods

Two types of data reduction methods for the analysis of low-energy electron diffraction intensity profiles and the extraction of surface atomic geometry have been proposed in recent years.[25-28] Since the general validity of these methods is currently under study, we shall only briefly outline the principles. The data reduction methods have their basis in the fact that kinematical (single-scattering) features of I-V profiles are generally predominant. Although the multiple-scattering features are rarely insignificant, it is argued that the effects of multiple scattering may be greatly reduced or eliminated by suitable averaging or transform procedures.

The first type of data reduction method involves the averaging of a large number of intensity profiles at constant momentum transfer $\underset{\sim}{S} = \underset{\sim}{k}' - \underset{\sim}{k}$. It is well-known that the kinematical scattering intensity is a function only of the energy E and $\underset{\sim}{S}$, while the multiple scattering involves intermediate scattering variables and is not simply a function of $\underset{\sim}{S}$ and E. It is therefore proposed that averaging the intensity over a suitable diffraction parameter (such as the azimuthal angle), which keeps $\underset{\sim}{S}$ and E constant, will retain the kinematical peaks in the intensity profiles while averaging out the dynamical features. One would then extract the surface atomic geometry from trial calculations using a fitting procedure with the relatively simple kinematical theory.[25-26] Lagally et al. have applied such a method in the analysis of data from Ag(111) and Ni(111) and their results demonstrate the kinematical appearance of the averaged profiles.[29,30] As emphasized by Duke and Smith and Pendry, however, the

central question is whether the resulting smoothed curves are sufficiently kinematical in character to be useful for accurate surface structure determinations. This question has yet to be fully explored.

The second type of data reduction method uses the Patterson function [27-28] or Fourier transform of the intensities $I_{hk}(S)$, where (hk) denotes a given diffraction beam and S is the momentum transfer in the direction normal to the surface. In low-energy electron diffraction applications these transforms take the form of a complex function:

$$P(x,y,z) = \sum_{h,k=-\infty}^{\infty} \int_{0}^{\infty} I_{hk}(S) \exp[2\pi i(hx + ky + Sz)]\, dS \qquad (16)$$

Each point (x,y,z) in the space represents a position vector connecting two scattering centers translated to an arbitrary common origin, and local maxima in P essentially correspond to probable locations of scattering centers providing data truncation errors and dynamical scattering do not introduce anomalous peaks. Clarke *et al.*[27] have used a real cosine transform to examine the structure of the Pt(100) surface. Buchholz *et al.*[28] have applied a transform method to low-energy electron diffraction data from Ni(111) with the conclusion that transforms of individual low-energy electron diffraction profiles taken at different diffraction geometry (e.g., different angles of incidence) are not the same, but transforms of averaged low-energy electron diffraction data give expected autocorrelation functions. Their conclusion points to a central problem with the use of transform methods in low-energy electron diffraction, namely that the available range in S may not be sufficiently large to eliminate data truncation errors and the effects of multiple scattering. Nevertheless,

if these difficulties are surmounted the transform method offers the advantage of being a fast, automated procedure for surface structure analysis.

2.3 Recent Analyses of Clean and Overlayer Systems

In this section recent applications of microscopic low-energy electron diffraction theory to the structure analysis of clean and simple overlayer systems are described. The data reduction procedures of intensity averages or transforms have not as yet been extensively applied and will not be discussed here. Although the analysis of clean surfaces appears to be in a rather satisfactory state of development, we shall see below that the extension to adsorbed overlayer systems has met with several difficulties. Specifically, disagreements between theoretical analyses have arisen as to the structures, both in a qualitative and quantitative sense, of certain overlayer systems. However, these contradictory analyses used independent sets of experimental data and discrepancies between the data are seemingly a major source of the difficulty. We do not judge these problems to be fundamental but rather regard them as temporary set-backs in the rapidly developing methodology of surface crystallography via low-energy electron diffraction.

The analysis of clean crystal surfaces has provided the testing ground for microscopic low-energy electron diffraction theories. Work has generally centered on the analysis of low-index faces of clean metals - namely, aluminum, copper, nickel, and silver. The importance of systematic studies over a wide range of incident angles and diffracted beams has been emphasized in order to examine the sensitivity and range

of applicability of model calculations. Such studies have been recently carried out for nickel [20,35,36] and copper [34]. As discussed in Section 2.2, current theories employ reasonably accurate descriptions of both the elastic electron-ion-core scattering and inelastic electron-electron collisions as well as making approximate provisions for the effect of lattice vibrations. Figure 5 is representative of the kind of agreement achieved in recent model calculations [20] on clean metal surfaces. One notes the good agreement between theory and experiment in terms of peak positions, peak widths, and the angular evolution of the I-V profiles. The agreement in terms of absolute reflectivities and relative peak heights is less satisfactory but certainly adequate. Indeed, uncertainties in the experimental data and models of the electron-solid potential limit the general agreement in peak positions to within 2-4 eV and peak intensities to within approximately 50%. The precision in peak positions should allow the determination of atomic distances to within approximately 0.1 Å. The peak heights and shapes can also be greatly affected by small changes in atomic positions, thereby providing an additional criterion for optimizing trial surface structures.

The structures of the uppermost atomic layers of the low index faces of aluminum, copper, and nickel appear to be very similar to the bulk structures. The intensity patterns exhibit the two-dimensional unit cells expected from the termination of the bulk structure. Nevertheless, several researchers have investigated the possible expansion or contraction of the outermost atomic layer in the direction normal to the surface. For the (100), (110), and (111) faces of nickel and for the (100) and (111) faces of copper, the outer layer spacing was found to be equal to the bulk

interplanar spacing to within 5%. Similar conclusions hold for the (100) and (111) faces of aluminum but the outer layer of the (110) face of aluminum is apparently contracted or moved inward 10-15% relative to the bulk spacing.[33] The more challenging cases of the reconstruction of clean surfaces such as occur for Pt(100) and Si(111) will no doubt be thoroughly studied with the attainment of extensive experimental intensity data on these systems.

The most interesting and technologically relevant applications of low-energy electron diffraction theory have been to the analysis of ordered adsorbate-substrate or "overlayer" systems. Such ordered overlayers may be formed, for example, by the introduction of foreign gas atoms or molecules to the surface of an initially clean single crystal. As discussed in Section 2.1, these overlayer structures are very often characterized by a two-dimensional lattice periodicity different from that of the underlying substrate, thereby leading to the occurrence of additional spots in the diffraction patterns. Model analyses have presently been applied to low-coverage coincidence structures. For these cases the adsorbed overlayer atoms are usually regarded as lying in a plane above an undistorted substrate lattice, and the problem reduces to that of determining the vertical and horizontal registry of the overlayer with respect to the substrate.

Several such analyses have recently been reported, most claiming accuracy to within 0.1 Å in adsorbate substrate distances.[38-44] Andersson and Pendry[38] examined the Ni(100) - c(2 x 2)-Na system with the conclusion that the Na atoms occupy four-fold coordinated sites at a distance of 2.87 Å above the topmost Ni layer.[39] Forstmann et al. reported an analysis

of the Ag(111) - ($\sqrt{3}$ x $\sqrt{3}$)R30° - I structure with the conclusion that the iodine atoms occupy three-fold sites a distance 2.25 Å above the topmost silver layer. Demuth et al.[40] have examined the c(2 x 2) overlayer structures of O, S, Se, and Te on Ni(100) finding the adsorbate atoms to occupy four-fold coordinated bonding sites at displacements of 0.90, 1.30, 1.45, and 1.90 Å, respectively, from the center of the top layer of nickel atoms. Andersson et al.[41] claim a similar structure for the oxygen on nickel system but place the oxygen atoms at 1.5 Å above the nickel layer in variance with the results of Demuth et al. Finally, Duke et al.[42] suggest that the oxygen-nickel structure is a four-fold coordinated reconstructed square overlayer with both Ni and O atoms lying in the range of 1.75 - 1.90 Å above the Ni substrate. Thus, considerably different structures have been proposed for the Ni(100) - c(2 x 2) - O system. Similar problems have arisen in the analysis of the Ni(100) - c(2 x 2) - S system.[40,43] However, in both of the above cases, different researchers analyzed different sets of experimental data. The data were sufficiently different to cause the differing conclusions. These results, of course, point to the need for a large base of reproducible intensity data for such overlayer systems before accuracy can be achieved in terms of absorbate-substrate distances.

3. CLASSIFICATION OF SURFACE STRUCTURES

3.1 The Structure of Clean Unreconstructed and Reconstructed Solid Surfaces

Surface reconstruction is defined as the state of the clean surface when its low-energy electron diffraction pattern indicates the presence of a surface unit mesh that is different from the bulk-like (1 x 1) unit mesh that is expected from the projection of the bulk x-ray unit cell. Conversely, an unreconstructed surface has a surface structure and a (1 x 1) diffraction pattern that is expected from the projection of the x-ray unit cell to that particular surface. Such a definition of surface reconstruction does not tell us anything about possible changes in the interlayer distances between the first and the second layers of atoms at the surface by contraction or expansion in the z-direction perpendicular to the surface that can take place without changing the (1 x 1) two-dimensional surface unit cell size or orientation. Indeed, several low Miller index surfaces of clean monatomic and diatomic solids exhibit unreconstructed surfaces, but the surface structure also exhibits contraction or expansion perpendicular to the surface plane in the first layer of atoms.

Over the past several years the intensities of the various low-energy electron diffraction beams have been measured for clean aluminum,[45] nickel,[46] silver,[47] copper,[48] and tungsten surfaces, as well as for lithium fluoride.[49] In all of these studies, low Miller index (100), (110), or (111)) crystal faces have been investigated. Using these experimental intensity data, calculations have been performed to determine the position of surface atoms based on theories in which the only adjustable parameters are the

atomic positions at the surface. Diffraction beam intensity data is available for several other monatomic and diatomic solids, but with these the structure analysis has been lacking. The calculations indicate x-ray unit cell to within 5% of the interatomic distance for atoms in the aluminum(100) and (111) and copper(100) and (111) crystal faces as well as for nickel(100),(110), and (111) crystal faces. These calculations can determine the atomic position in the surface layer within 0.1 Å. However, the (110) face of aluminum was found to be contracted by about 10-15% from the bulk interlayer spacing.[33] The best agreement between calculations and experimental intensities for Al(110) are obtained when the surface atoms are allowed to move closer to the second layer. Since the aluminum(110) crystal face is of somewhat lower atomic density than the (111) or (100) crystal faces, this observation may signify a trend that would indicate that surface rearrangement without reconstruction by expansion or contraction of atoms in the z-direction may take place in more open crystal faces while such an occurrence is not likely in high density, low surface free energy crystal faces.

Similar changes in the interlayer spacing have been calculated by Laramore and Switendick for the (100) face of lithium fluoride.[50] According to their calculations, the top lithium and fluoride ion sublayers were separated by about 0.25 Å. The lithium ion sublayer appears to be contracted by a greater amount towards the bulk. Low-energy electron diffraction experiments indicate that various alkali metal halide (100) surfaces have the (1 x 1) surface structure that is expected from the projection of the x-ray unit cell.[51] However, Gallon et al. have shown that the stoichiometry of the alkali metal halide at the surface may be very different from the

composition in the bulk. There may be surface excess of either the alkali metal atom or the halogen. While such changes do not seem to affect the unit cell size at the surface, this non-stoichiometry may be responsible for the magnitude of the contraction of the sublayers at the surface. The change of interatomic distance at alkali-halide surfaces have been calculated by Benson et al.[52] and others without the need of assuming non-stoichiometry. However, the magnitude of their predicted values are different from those calculated in the low-energy electron diffraction analysis of Laramore and Switendick. Low-energy electron diffraction studies of the surface structure of lithium hydride by Holcomb et al.[53] indicated that the composition at the surface is different from that of the bulk composition. There is evidence of precipitation of the alkali metal on the alkali hydride surface. During these chemical changes, however, the surface diffraction pattern remained characteristic of (1 x 1) unreconstructed surface structure. Thus, it appears that at least for alkali halides the surface free energy is lowered by the introduction of excess defects, positive or negative ion vacancies, that will change the chemical composition and result in a marked non-stoichiometry in the surface layer. In this way the surface free energy is to be lowered more than by suitable reconstruction of the surface by which atoms occupy new equilibrium positions. The surface free energy, of course, may also be lowered by changes of interatomic distances perpendicular to the surface plane. We will observe a combination of these effects on these unreconstructed ionic crystal surfaces. It is expected that compound semiconductors, those formed from elements in the II-VI and III-V groups of the periodic table, may also show similar effects.[54] There are

several cases where both the surface composition and the surface unit cell changes simultaneously. These changes that appear on various oxide surfaces will be discussed below.

3.1.1 Surface reconstruction

There are several low Miller index surfaces that exhibit reconstruction, i.e., the surface unit mesh is different from the usual bulk-like (1 x 1) mesh.[55] These reconstructed surfaces are the silicon (111), (100), and (110),[56,57] the germanium (111), (100) and (110) surfaces,[56] the diamond (111),[58] the platinum (100) and (110),[59] the gold (100) and (110),[60] and iridium (100) and (110) surfaces,[61] the bismuth $(11\bar{2}0)$,[62] the antimony $(11\bar{2}0)$,[62] and the tellurium (0001) crystal faces.[63] Various diatomic solids, the gallium arsenide(111),$(\bar{1}\bar{1}\bar{1})$ crystal faces,[64] the gallium antimonide(111) and $(\bar{1}\bar{1}\bar{1})$,[64] as well as the cadmium sulfide[65] and zinc oxide(0001)[66] faces and oxides under suitable conditions, i.e., vanadium oxide,[67] aluminum oxide,[68] and barium titanate,[69] also exhibit surface reconstruction.

One of the most detailed studies of surface reconstruction was carried out on the silicon(111) surface.[70] Upon cleaving at 25°C, the surface exhibits a (2 x 1) surface structure. On heating to about 300-400°C, the surface structure changes, according to Mönch, the (2 x 1) structure converting to the (7 x 7) structure. The (7 x 7) structure is then the stable structure of the (111) crystal face. Joyce,[71] however, reported that in the presence of trace impurities, such as iron or nickel, the (2 x 1) surface is converted first to a (1 x 1) structure at 400°C, and the (7 x 7) structure forms only upon heating to 700°C. There is enough evidence to indicate that the temperature at which the impurity-stabilized (1 x 1) surface structure transforms into the (7 x 7)

structure depends markedly on the amount and the nature of the trace impurities on the surface.

There are several theories that can explain surface reconstruction in the absence of any major change in chemical compositon at the surface. Taloni and Haneman[72] showed that relaxation of surface atoms out of the surface plane increases the overlap of localized electron orbitals, thereby lowering the surface free energy. Trullinger and Cunningham[73] proposed that the softening of phonon modes at the surface gives rise to the periodic relaxation of surface atoms. All of these models indicate that surface reconstruction is indeed possible and results in a lowering of the surface free energy, but they do not predict the unique surface structure that is likely to be most stable. Since transformation from one surface structure to another can take place on both silicon and germanium surfaces as a function of temperature, the magnitude of the surface energies associated with the two structures are within kT of each other. Such a small energy difference should make it difficult to predict the relative stability.

Among metals, the most consistent changes of the surface structure were observed for the (100) crystal faces of three 5d transition metals that are neighbors in the periodic table. These metals are gold, platinum, and iridium. All three metals exhibit the so-called (5 x 1) surface structure that is shown in Figure 6. There are two perpendicular domains of this structure, and there are 1/5, 2/5, 3/5 and 4/5 order spots between the (00) and (10) diffraction beams. The surface structure is not quite as simple as the short-hand notation indicates as is shown by the splitting of the fractional order beams. The surface structure

appears to be stable at all temperatures from 25°C to the melting point although at elevated temperatures impurities from the bulk can come to the surface and cause a transformation of this structure to the impurity stabilized (1 x 1) surface structure.[59] Carbon at the surface that may diffuse out of the bulk in minute quantities or adsorbed gases of various types, CO, C_2H_2, etc., can cause the surface atoms to relax back to their bulk-like (1 x 1) atomic positions.[59] The diffraction beam intensities of the (5 x 1) structure are under close investigation in many laboratories.

Preliminary calculations by Clarke et al.[27] and in this laboratory indicate that a model for Pt(100) in which the surface atoms assume a distorted hexagonal configuration by out-of-plane buckling is favored. The apparent (5 x 1) unit cell is then the result of coincidence of the atomic position of atoms in the surface, i.e., in the distorted hexagonal layer, with atoms of the undistorted second layer below. Surface atoms in any crystal face are in an anisotropic environment which is very different from that about bulk atoms. The crystal symmetry that is experienced by each bulk atom is markedly higher than for atoms placed on the surface. The change of symmetry and the lack of neighbors in the direction perpendicular to the surface permit displacements of the surface atoms in ways that are not allowed in the bulk. Surface relaxation can give rise to a multitude of surface structures depending on the electronic structure of a given substance. It is indeed surprising that there are so many solid surfaces that do not exhibit surface reconstruction. The adsorption of gases, such as oxygen or hydrogen, or the presence of impurities that segregate on the surface from the bulk, may cause or inhibit surface reconstruction as indicated by many recent experiments.

Changes of chemical compositon at the surface can produce marked changes in surface structure and cause the formation of a new surface unit cell. The (0001) crystal face of Al_2O_3 has been studied by several researchers. Upon heat treatment to elevated temperature there is an apparent reconstruction of the surface oxides evidenced by the formation of a new diffraction pattern that is accompanied by oxygen evolution.[68] In ultra-high vacuum such heat treatment has resulted in the transformation of the (1 x 1) surface structure to one characterized by a $(\sqrt{31} \times \sqrt{31})R \pm 9°$ unit mesh. Structural rearrangement was accompanied by the loss of oxygen; therefore, it has been interpreted as an oxygen-poor or a reduced oxide surface structure. The structural transformation is reversible, however, depending either on the partial pressure of oxygen or on the presence of excess aluminum on the surface. The complex surface structure whose formation is observed can be explained assuming the formation of AlO or Al_2O at the surface. Fiermans and Vennik reported on some interesting observations on vanadium pentoxide.[67] Under the influence of the low-energy electron beam incident on the surface, the transformation of $V_2O_5(010)$ to $V_{12}O_{16}(010)$ was observed in the surface layer accompanied by the loss of oxygen. They have demonstrated that this proceeds by domain formation on the surface and the two different structures $V_{12}O_{16}(010)$-(4 x 1) and $V_{12}O_{16}(010)$-(1 x 2) are involved depending on the degree of non-stoichiometry of the sample. Studies of Szalkowski et al. have confirmed that the surface of V_2O_5 is unstable and it is reduced in vacuum.[74] There are lower oxides, $VO_{0.9}$, V_2O_3 and VO_2 that retain their surface composition which is the same as that of bulk composition within the experimental accuracy (5%).

Aberdam and coworkers [69] have observed the diffraction pattern from the (001) face of barium titanate, $BaTiO_3$, prepared by different heat treatments. Near 1120°K the (1 x 1) mesh is noted which changes after a long period to the ($\sqrt{3}$ x $\sqrt{3}$) structure. The surface arrangement is considered to be due to the ordering of vacancies at the surface. A hysteresis in the temperature curve was found between 370-700°K and this could be associated with a cubic-tetragonal surface phase transition.

So far, we have noted three examples in which the reduction of the surface oxide causes a change of surface structure and surface unit cell. The effect of the reverse process, oxidation, has caused similar rearrangement. Oxidation of nickel and other metal surfaces may cause reconstruction of the surface layer and the surface layer is then characterized by a mixed layer containing both oxygen and metal atoms although the evidence is still circumstantial as to the chemical character of the structure of the reconstructed layer. Most experiments indicate that such a rearrangement is likely to take place during highly exothermic surface reactions such as oxidation, nitridation, or during the formation of carbides.

3.1.2 Stepped, high Miller index surfaces

Low-energy electron diffraction studies have been applied, in general, to study the surface structure of close-packed faces of solids of low Miller index. These surfaces are chosen for structural investigation since they have the lowest surface free energy, and they are therefore stable with respect to rearrangement of crystal faces or to disordering up to or near the melting point. Studies of surfaces of high Miller index and higher surface free energy are important in their own right. It is

Figures 8A - 8D. The terrace width is calculated from the doublet separation while the step height is obtained from the variation of the intensity maximum of the doublet diffraction beam features with electron energy. Let us consider the analysis of these diffraction patterns.

Several approaches are available in the literature, all kinematic and all yielding the same results. Henzler,[78] extending the derivation by Ellis and Schwoebel,[76] has shown that the scattered intensity, I, at an angle ϕ with electron beam incidence normal to the terraces is given by

$$I = \text{constant} \cdot \frac{\sin^2[\frac{1}{2}k \cdot a(N+1)\sin\phi]}{\sin^2[\frac{1}{2}k \cdot a\sin\phi]} \times \sum_{i=-\infty}^{+\infty} \delta[\tfrac{1}{2}k(N \cdot a + g)\sin\phi + \tfrac{1}{2}kd(1+\cos\phi) - i\pi] \qquad (17)$$

where the terrace has $(N + 1)$ rows, $k = 2\pi/\lambda$, $\underline{a}$ is the separation of the atomic rows, $\underline{d}$ is the step height, and $\underline{g}$ is the horizontal shift of one terrace compared to that below it. The first term is the intensity distribution for a grating of $(N + 1)$ slits and the maxima are given by the Bragg equation

$$\tfrac{1}{2}k \cdot a\sin\phi = n\pi \quad . \qquad (18)$$

The second term in the sum of δ functions with a separation $\Delta\phi$ given (near $\phi = 0$) by $\Delta\phi = \lambda/(Na + g)$, in other words, dependent only on the width and the displacement of the terraces. When two delta functions fall on a maximum of the intensity curve, a doublet arises and when only one delta function falls on the maximum of the intensity function, a singlet is observed. The delta functions converge towards the specular reflection of the high-index plane. The spot pattern itself, however, converges

important to elucidate their atomic structure and stability under a variety of experimental conditions in the presence of reactive and inert gases and in vacuum.

The earliest diffraction observation from a high index surface is probably that of niobium.[75] The first detailed study of a stepped surface of this type is that of Ellis and Schwoebel.[76] They had examined a uranium dioxide, UO_2, crystal cut at 11.4° from the (111) plane in the (112) zone. Heating this sample at 1100°K in ultra-high vacuum for one hour produces a diffracton pattern resembling that from a UO_2(111) crystal face except that the spots were elongated and appeared to be split into multiplets. Heating at 1200°K in 10^{-7} torr oxygen generated a pattern with each (111) spot resolved into a well-defined doublet at certain electron energies. This behaviour with doublets appearing in place of single spots characteristic of a terrace geometry has been reported for all of the stepped surfaces examined. Recent low-energy electron diffraction investigations of copper,[77] germanium,[78] gallium arsenide,[78] and platinum surfaces[79] indicate that the surfaces of crystals characterized by high Miller index consist of terraces of low index planes separated by steps often one atom in height. The ordered stepped surfaces displayed varying degrees of thermal stability. Figure 7 shows one crystallographic zone of a face-centered cubic crystal. The circles indicate the direction and angle of cut of the various high Miller index surfaces and Table I indicates the Miller indexes associated with these crystal surfaces. The diffraction patterns that are obtained from the various high miller index surfaces and the surface structure that can be derived from these diffraction patterns are indicated in

towards a (00) spot of the terrace plane. It has been shown that the separation of the doublet is inversely proportional to (Na + g), the terrace width, which is therefore easily determined. Also, the step height can be found from

$$V_{00(\text{singlet max})} = \frac{150}{4d^2} s^2 \qquad (19)$$

where V_{00} are the voltages where a singlet of maximum intensity is observed, $\underline{d}$ is the step height and $\underline{s}$ is an integer. This method has been applied to the determination of step height by Henzler[80] and by Joyner, Lang, and Somorjai.[79] The diffraction patterns to be expected from stepped surfaces have also been examined using laser simulation by Campbell and Ellis,[81] who have shown that the single scattering diffraction pattern is potentially very informative. The terrace width does not have to be very precise to obtain satisfactory diffraction patterns. Houston and Park,[82] in a theoretical study, have shown that there may be a great deal of uncertainty in the step width. All that is needed is that on an average the step width is well-defined to obtain a diffraction pattern of satisfactory quality. That is, if the diffraction pattern indicates that the terrace width is 6 atoms wide, this does not rule out the presence of a large number of terraces 4,5, 7 or 8 atoms wide. Since the rearrangement of high Miller index surfaces to ordered low index terraces separated by step takes place regardless of the chemical bonding in the crystal, it may be regarded as a general structural property of high index surfaces. It is therefore of value to have a standardized nomenclature to identify stepped surface structures. Stepped surfaces are indicated by the postscript S so that Pt(S) indicates a stepped

platinum crystal surface. The ordered step array can then be completely designated by the width and the orientation of the terraces and the height and the orientation of the steps. Thus, a stepped surface may be designated as Pt(S)[m(111) x n(100)], where m(111) designates a terrace of (111) orientation and m atomic rows in width and n(100) indicates a step of (100) orientation and n atomic layers high. Pt(S)-[m(111) x (100)] indicates the structure of various high Miller index platinum stepped surfaces having step heights of one atomic layer. (The 1 is not shown in front of the step orientation.) A more detailed description of nomenclature of more complex stepped structures is given elsewhere.[79]

The thermal stability of the steps is of great interest; however, only a few studies have been directed to probe the high temperature structural properties of high Miller index surfaces. For semiconductors, where the surface is generated by cleavage, the steps may be removed at elevated temperature and faceting occurs. But, in metals, the stepped high index surfaces are found to be stable close to the melting temperature.

Perhaps the most significant property of stepped surfaces is their great reactivity as compared to low index crystal faces. The chemisorption of hydrogen, oxygen, and carbon monoxide was studied by low-energy electron diffraction on ordered stepped surfaces of platinum.[83] The stepped surfaces behave very differently during chemisorption from those of low index platinum surfaces, and the various stepped surfaces also behave differently from each other. Hydrogen and oxygen, which do not chemisorb easily on the (111) and (100) crystal faces of platinum, chemisorb readily at relatively low temperature on the stepped platinum surface.

In contrast to the ordered adsorption of CO on low index platinum surfaces, where several ordered surface structures have been detected, the adsorption is disordered on stepped surfaces, and there is evidence of dissociation of the molecule. Perhaps the best evidence of the enhanced reactivity of stepped surfaces comes from molecular beam studies on platinum surfaces. The hydrogen-deuterium exchange to form hydrogen deuteride, HD, was studied on (111) and stepped platinum surfaces.[84] While the scattering of both H_2 and D_2 was highly specular from the (111) crystal face and no HD signal could be detected at any surface temperature between 300-1000°K for any angle from the surface normal, HD is readily detected from stepped surfaces over this temperature range. Between 5-10% of the incident deuterium is converted to HD on a stepped surface with 9 atom wide (111) orientation terraces. It appears that at least on platinum surfaces the dissociation of large binding energy diatomic molecules takes place at steps or at least steps play a rate-determining role in the chemical process. The reactivity of stepped surfaces was also investigated during the chemisorption of various hydrocarbons on platinum surfaces. Aromatic and aliphatic hydrocarbons adsorbed on low index (111) and (100) platinum crystal faces without any apparent decomposition or dehydrogenation in the temperature range of 300-500°C.[85] Low-energy electron diffraction and work function change measurements both indicate that these molecules remain intact on the low index platinum surfaces. Therefore, their surface crystallography may be studied conveniently in this temperature range. The chemisorption of over 25 hydrocarbons has been studied by low-energy electron diffraction on four

different stepped crystal faces of platinum, the Pt(S)-[9(111) x (100)], Pt(S)-[6(111) x (100)], Pt(S)-[7(111) x (310)] and Pt(S)-[4(111) x (100)] structures.[86] These surface structures are shown in Figure 8. The chemisorption of hydrocarbons produces carbonaceous deposits with characteristics which depend on the substrate structure, the type of hydrocarbon chemisorbed, the rate of adsorption, and the surface temperature. Thus, in contrast with the chemisorption behaviour on low Miller index surfaces, breaking of carbon-hydrogen and carbon-carbon bonds can readily take place at stepped surfaces of platinum. Hydrocarbons on the [9(100) x (100)] and [6(111) x (100)] crystal faces form mostly ordered partially dehydrogenated carbonaceous deposits while disordered carbonaceous layers are formed on the [7(111) x (310)] surface, which has a high concentration of kinks in the steps. The distinctly different chemisorption characteristics of these stepped platinum surfaces can be explained by considering the interplay of four competing processes: (1) the nucleation and growth of ordered carbonaceous surface structures, (2) dehydrogenation, i.e., breaking of carbon-hydrogen bonds in the adsorbed organic molecules, (3) decomposition of the organic molecules, i.e., breaking of both carbon-hydrogen and carbon-carbon bonds at steps, and finally, (4) rearrangement of the substrate by faceting. On the [9(111) x (100)] and [6(111) x (100)] crystal faces, processes (1) and (2) predominate. On the [7(111) x (310)] face process (3) predominates, while process (4) is the most important on the [4(111) x (100)] face. The importance of atomic steps in surface chemical reaction on platinum

cannot be emphasized strongly enough. In many reactions the dissociation of large binding energy diatomic molecules is a rate-limiting step. Atomic steps appear to catalyze this process. The lack of reactivity of low Miller index surfaces in hydrocarbon reactions indicates the importance of steps in breaking carbon-hydrogen and carbon-carbon bonds so important in various surface reactions of hydrocarbons. The nucleation and growth of ordered carbon structures that appear only on stepped platinum surfaces are important in catalyzing complex structure-sensitive organic reactions such as isomerization and dehydrocyclization.[87] It appears that by cutting the right stepped surface one can produce prototypes of surfaces present on most catalysts under industrial conditions and using these well-defined, well-characterized stepped surfaces, one can establish correlations between chemical reactivity and surface structure under controlled conditions. It appears that stepped surfaces are more characteristic of the structure of real surfaces that participate in crystal growth or vaporization or surface chemical reactions. Hence, the electronic and atomic properties of stepped surfaces, their chemisorption and reactivity will be a topic of intense investigations in the future.

3.2 The Structure of Adsorbed Gases on Solid Surfaces

Much of the thrust of surface crystallography is aimed at understanding the structure of adsorbed gases on surfaces. Experimental information on the structure of adsorbed gases from low-energy electron diffraction studies has been accumulating rapidly since the late 1950's. Most of the experiments initially concentrated on the adsorbed structures formed

by monatomic and diatomic gases on low Miller index surfaces of monatomic solids.[88] The gas species, in most cases, has molecular dimensions which are smaller than the interatomic distances in the substrate. Only in a few recent instances, such as in the cases of oxygen, selenium, and sulfur adsorption on nickel(100) surfaces, have low-energy electron diffraction intensity analyses been used in efforts to identify the unique atomic positions of these adsorbed atoms or molecules on the surface as well as the distances of separation from the metal atoms. In the over two hundred surface structures that have been reported, the surface structures were identified only by viewing the diffraction pattern without making use of the intensities of the various diffraction beams. The diffraction pattern, of course, reveals the rotational symmetry and the size of the unit cell of the surface structure with respect to that of the substrate. This information, however, does not define a unique atomic site for each adsorbed species as the diffraction pattern may be assigned to several surface structures, all of them characterized by the same size and symmetry of unit cell. This section will be concerned only with a discussion of the surface structure of adsorbed gases as determined from the symmetry and separation of the diffraction beams in the diffraction pattern. The discussion will be restricted to gases that do not undergo chemical reactions on and with the substrate. Thus, the adsorbed structure observed on stepped surfaces will not be discussed but the papers that discuss the structures of these partially dissociated organic molecules adsorbed on stepped surfaces are referred to in the previous section. Such chemical reactions are quite common and may

follow the chemisorption of oxygen, hydrogen, or other reactive molecules. We shall discuss the surface structure of adsorbed gases on low Miller index surfaces in two parts. First, the surface structures of small molecules will be discussed, and then in a separate section the surface structures of adsorbed hydrocarbons, large aliphatic and aromatic molecules will be reviewed.

3.2.1. Principles of ordered adsorption

Practical studies of adsorption require surface coverage of the adsorbed gas that is greater than about 5% of the number of available surface sites, which is approximately 10^{15} atoms/cm^2 under the conditions of most experiments.[55] The coverage, σ, is determined primarily by the residence time, τ, of the incident atoms or molecules and by the incident flux, F,

$$\sigma = \tau \cdot F \quad . \tag{20}$$

The flux is given by

$$F\left(\frac{\text{molecules}}{\text{cm}^2\text{sec}}\right) = 3.52 \times 10^{22} \frac{P_{\text{torr}}}{(MT)^{1/2}} \tag{21}$$

using the kinetic theory of gases, while the residence time can be expressed as

$$\tau = \tau_0 \exp[\Delta H_{ads}/RT] \ , \tag{22}$$

where P is the vapor pressure and ΔH_{ads} is the heat of adsorption. τ_0 is related to the period of a single surface atom vibration, and the other symbols have their usual meanings. Frequently, $\Theta = \sigma/\sigma_0$, the degree

of covering, is defined in discussing the properties of the adsorbed layers where σ_0 is the number of surface sites available for adsorption. The experimental conditions are adjusted by manipulation of the flux or the temperature to obtain measurable adsorption rates or coverages. The heat of adsorption depends on the coverage and therefore it is customary to define

$$\Delta H_{ads}^{diff} = \left(\frac{d\Delta H_{ads}}{dN}\right)_T , \qquad (23)$$

where ΔH_{ads}^{diff} is the increase in the heat liberated by the adsorption of an additional amount of gas, dN. Recently, work function measurements and ellipsometry have been used to obtain the differential heats of adsorption as a function of coverage using single crystal surfaces. Such measurements reveal the nature of the molecular interaction in the adsorbed layer, whether it is attractive or repulsive. The ordering of rare gases, xenon and argon, which have low heats of adsorption (2-8 kcal/mole) have been studied successfully in the temperature range of 10-78°K. On the other hand, most molecules that chemisorb, i.e., have high heats of adsorption ($\geq$ 15 kcal/mole), can be studied readily at 300°K and even at low gas pressures that are commonly used in low-energy electron diffraction studies ($< 10^{-4}$ torr).

Ordering of the molecules on the surface requires that the adsorbed species have sufficient mobility[89]; thus, the adsorbed molecules have to be able to overcome the activation energy, ΔE_D, that is associated with surface diffusion. Fortunately, the heat of adsorption, ΔH_{ads}, is in general greater than ΔE_D by at least a factor of two in most cases, so that the coverage remains relatively unchanged while surface ordering proceeds.

Indeed, two-dimensional gas-liquid-solid transitions are possible because the adsorbed layer is now protected from desorption or diffusion into the bulk by large activation energy barriers for many of the systems of interest. It has also been found that suitable impurities adsorbed on surfaces can reduce the activation energy of surface diffusion so that ordering may commence in the presence of certain catalysts at lower temperatures. Low-energy electron diffraction studies of ordering as a function of coverage have detected order-disorder transitions that were likened to liquid-solid transitions in two dimensions as a function of coverage and temperature. Disordered adsorption at low coverages can be followed by ordering with increasing coverage as the motion of the molecules in the adsorbed phase becomes restricted. In order to overcome the decrease in entropy that is associated with the formation of the ordered layer on the surface, there is likely to be a large heat of ordering (exothermic) similar to the heat liberated in freezing a liquid. If the attractive interaction between the adsorbed molecules is large, ordered islands of the adsorbate may appear at low coverages. If the attractive interaction between the adsorbed molecules is weak compared to RT, the thermal energy at the temperature of the experiment, the adsorbed layer remains disordered. Ordering of these disordered layers may be controlled by changing the temperature of the substrate and/or changing the coverage. In general, the important system parameters that control ordering are the heat of adsorption as a function of coverage and the activation energy of surface diffusion, while the important experimental parameters are the coverage and the temperature.

3.2.2 The structure of small adsorbed molecules on low Miller index surfaces

The substrates that have been most frequently used in adsorption studies by low-energy electron diffraction were the highest atomic density crystal faces of monatomic solids with face-centered cubic or body-centered cubic crystal structure. These crystal faces also have the lowest surface free energies and are therefore the most stable. Tables II, III, and IV list the surface structures of small adsorbed gas molecules that have been reported. A previous compilation[90] was revised to include the over thirty new surface structures that were reported in the past two years. Surface structures of gases that were adsorbed on substrates with 2-fold, 4-fold, and 6-fold rotational symmetry are tabulated separately, since this classification permits useful correlation of the various structures. Inspection of these tables reveals that most of the surfaces are characterized by (1) the smallest unit cell permitted by the molecular dimensions and adsorbate-adsorbate and adsorbate-substrate interactions, and (2) the molecules adsorbed on the surface are likely to form ordered structures that have the same rotational symmetry as the substrate. These correlations were expressed as the rule of "close-packing" and the rule of rotational symmetry, and their judicious application permits the prediction of surface structures or surface units cells with a reasonable degree of accuracy. There are, of course, exceptions to these rules of ordering. These arise if there is a chemical reaction between the substrate and the adsorbed molecule. The presence of multiple binding states, detectable for example during the chemisorption of CO on several metal surfaces, also makes the application

of these simple rules difficult. It appears that for small molecules, whose dimensions are smaller than or similar in size to the interatomic distances in the substrate, violation of the rules of ordering is indicative of chemical interaction with the substrate that results in the formation of coincidence lattices with large apparent unit cells. It should be noted that such rules are either not applicable or rarely applicable to molecules whose size is greater than the interatomic distance in the substrate plane. These adsorbates may overlap several substrate atoms and their interaction with the substrate may be described only by a complex potential energy surface that contains contributions from many surface atoms. Also, in this case, the nature of the attractive interaction between the adsorbed molecules should play a more important role in determining the adsorbate structure. Thus, these surface structures will be discussed separately in the next section.

3.2.3 The structure of large adsorbed molecules on solid surfaces

The surface structure of adsorbed xenon has been studied on various substrate surfaces. Early evidence from studies of xenon adsorption on a graphite substrate[91] provided support for site adsorption by demonstrating the existence of $(\sqrt{3} \times \sqrt{3})$-R30° xenon structure at 90°K. At lower equilibrium surface coverages, fuzzy ring-like diffraction features were observed and were considered as indicative of close-packed arrangement. Palmberg[92] has examined the adsorption of xenon on palladium(100) at 77°K in combination with work function measurements and Auger electron spectroscopy. Again, extra diffraction features appear only as the monolayer coverage is reached and the xenon structure has the symmetry of the substrate with

unit cell vectors parallel to those of the underlying metal. The unit cell size is, however, not related to the palladium unit cell and yields a xenon-xenon spacing of 4.4 Å, close to the solid xenon value of 4.37 Å. The packing of the physically adsorbed layer is therefore dominated by the xenon-xenon attractive interaction. Xenon adsorption on the (100) crystal face of copper at 77°K was studied by Chesters and Pritchard[93], who again observed disorder at low coverages giving way to domains of ordered xenon at close to the monolayer. Here the physically adsorbed layer has 6-fold symmetry rather than the 4-fold symmetry of the (100) copper substrate and the xenon-xenon distance of 4.5 ± 0.1 Å is found. Ignatiev et al.[94] have demonstrated the growth of ordered (111) orientation xenon films on an iridium(100) substrate. Thus, it appears that regardless of the substrate structure and rotational symmetry, xenon forms a (111) orientation overlayer on the various substrate surfaces. Similar results were obtained in a systematic study by Dickey et al.[95] at 8°K where ordered structures were reported for the physical adsorption of argon and neon on the (100) plane of niobium.

Low-energy electron diffraction and work function change studies of the adsorption of a large number of substituted aromatic molecules were carried out by Gland and Somorjai[85,96] on the (111) and (100) crystal faces of platinum. These studies were carried out at low pressures (10^{-9} - 10^{-7} torr) and at temperatures of 20-300°C. After adsorption, reorientation of the molecules in the adsorbed layer is necessary to form the ordered structures. Molecules that have either higher rotational symmetry, mesitylene for example, or have only small size substituents on the benzene rings, exhibit better ordering if the adsorption is carried

out at low incident flux. The adsorbed layers are more ordered on the (111) crystal face than on the (100) crystal face of platinum. The work function changes upon adsorption range from -.3 eV for cyclopentane to -2.7 eV for pyridine. The surface structure and the corresponding work function changes that were observed during adsorption are shown in Table V. Both the diffraction and work function change data indicate that, under the conditons of these experiments, all of the molecules chemisorb with their benzene ring parallel to the surface and interact with the metal surface primarily via the π electrons in the benzene ring. The substituent groups play an important role in determining the ordering characteristics of the overlayer but do not markedly affect the strength of the chemical bond between the substrate and the absorbate. An interesting case history of change of chemical bonding with increasing coverage is that of benzene adsorbed on Pt(111). Benzene first forms a disordered layer on the Pt(111) surface but with further exposure, the Pt(111)-$\begin{pmatrix} -2 & 2 \\ 4 & 4 \end{pmatrix}$- benzene structure is formed. (We use matrix notation in terms of the vectors of the substrate mesh.) Continued exposure results in the transformation of the surface structure to another ordered surface structure Pt(111)-$\begin{pmatrix} -2 & 2 \\ 5 & 5 \end{pmatrix}$. The first structure forms shortly after the minimum in the work function change has been reached, $\Delta\phi$ =-1.4 volts. After the minimum has been passed, the work function change increases toward a steady state value of -0.7 volts. The second ordered structure $\begin{pmatrix} -2 & 2 \\ 5 & 5 \end{pmatrix}$, forms when the work function change is about -1.1 volts. This correlation between the transformation of the benzene surface structure and the change in the work function suggests that the orientation of the adsorbed benzene molecules is changing markedly as a function of increased exposure.

A decrease in the density of the adsorbed layer during the order-order phase transformation is not possible because of the high flux that is continuously incident on the crystal throughout the experiment. In fact, the density of the adsorbed layer is increasing during continued exposure as indicated by the observation that higher incident benzene flux causes the transformation of one benzene surface structure to another to occur more rapidly. The work function change indicates that there is a decrease in the magnitude of the charge transfer occurring as the density of the adsorbed layer increases. If the adsorbed species has the same bonding characteristics during the transformation and the coverage increases, the work function would be further decreased. Thus, the increasing density accompanied by a decreasing magnitude of work function change can only be explained by assuming the area of the adsorbed molecule must be decreasing. A likely model consistent with these criteria is that initially benzene is adsorbed with its ring parallel or at a small angle to the surface. The final adsorbed state may involve reoriented benzene molecules adsorbed with their rings at a large angle or perpendicular to the surface. The initial adsorbed species would be held on the surface by π bonds of the aromatic ring similar to the bonds in the so-called sandwich compounds. Since the metal surface is highly electron deficient, a large induced dipoled would be expected in the adsorbed layer. The second structure that forms at large exposures may involve benzene molecules adsorbed with their rings perpendicular to the surface. For this type of adsorption to occur, the benzene must either lose a hydrogen to form a σ bond, or its aromaticity. Recent exchange studies between deutero-benzene and benzene on platinum films have shown rapid exchange of hydrogen and deuterium between these species.[100] These workers postulate loss of

hydrogen in benzene without loss of aromaticity to form a singly bonded adsorbed species. Thus, the adsorbed species that gives the second $\begin{pmatrix} -2 & 2 \\ 5 & 5 \end{pmatrix}$ structure is most likely a singly dehydrogenated benzene molecule covalently bonded to the surface. This type of reorientation satisfies both criteria for the surface transformation, that is, the surface area occupied by the adsorbed species decreases and the amount of charge transfer decreases as well. Low-energy electron diffraction and work function changes indicate that pyridine bonds primarily through its nitrogen to the platinum surface. The corresponding work function change is very large, of the order of -2.5 eV. Napthalene forms a very well-ordered Pt(111)-(6 x 6) napthalene structure when adsorbed on the (111) surface at 150°C and the work function change upon adsorption is about -2.0 eV. Both the surface structure structure and the work function change on adsorption of napthalene indicates that the napthalene molecules lie parallel to the platinum surface and π bond to the metal substrate. Another interesting study was the low-energy electron diffraction and work function investigation of the adsorption of cyclohexane, cyclohexene and cyclohexadiene on the platinum(111) and (100) surfaces.[97] Both the surface structural and the work function change data can be correlated to the various chemical bonds that these saturated and partly dehydrogenated molecules form with the metal surface. Both cyclohexane and cyclohexene adsorb on the metal surface without strong chemical interaction that would lead to dehydrogenation. These molecules stay intact and their structural characteristics can be rationalized from their molecular geometry and bonding abilities. Cyclohexane forms a single σ bond while cyclohexene π bonds through its olefinic double bond to the platinum

surface. Cyclohexadiene appears to be unstable on platinum surfaces. Its dehydrogenates rapidly at 25°C and the surface structures that form are those characteristic of benzene.

Studies of the surface structure and chemical bonding of organic molecules to various solid surfaces is an important field that underlies the phenomena of adhesion and lubrication. Future studies in this field will be extended to larger organic molecules of greater complexity. It appears that detailed studies of molecular crystals of various types to determine the surface structure and surface crystallography can also be carried out. As surface structure analysis using the diffraction beam intensities allows routine determination of the surface structures of small molecules, surface crystallography will turn to more complex structures. Such development is certainly expected during the next decade.

Acknowledgements

This work was carried out under the auspices of the U.S. Atomic Energy Commission. The financial support of the National Science Foundation and the Petroleum Research Foundation of the American Chemical Society is gratefully acknowledged.

References

1. E. A. Wood, J. Appl. Phys., 35, 1306 (1964).
2. See, for example, C. Kittel, Introduction to Solid State Physics, 4th ed., (John Wiley & Sons, Inc., New York, 1971).
3. P. J. Estrup and E. G. McRae, Surface Sci., 25, 1 (1971).
4. R. L. Park and H. H. Madden, Jr., Surface Sci., 11, 188 (1968).
5. N. F. Mott and H. S. W. Massey, The Theory of Atomic Collisions. (Oxford University Press, London, 1965).
6. J. J. Lander, in Progress in Solid State Chemistry, Vol. 2 (Pergamon, New York, 1965).
7. E. G. McRae, J. Chem. Phys. 45, 3258 (1968); Surface Sci. 8,14 (1967).
8. D. S. Boudreaux and V. Heine, Surface Sci. 8, 426 (1967).
9. K. Kambe, Z. Naturforsch. 22a, 422 (1967).
10. J. L. Beeby, J. Phys. C 1, 82 (1968).
11. C. B. Duke and C. W. Tucker, Jr., Surface Sci. 15, 231 (1969).
12. J. B. Pendry, J. Phys. C. 2, 2273 (1969); J. Phys. C 2, 2283 (1969).
13. D. W. Jepsen, P. M. Marcus, and F. Jona, Phys. Rev. Lett. 26, 1365 (1971); Phys. Rev. B 5, 3933 (1972).
14. J. A. Strozier and R. O. Jones, Phys. Rev. B3, 3228 (1971).
15. G. Capart, Surface Sci. 26, 429 (1971).
16. C. B. Duke and G. E. Laramore, Phys. Rev. B2, 4765 (1970).
17. See, for example, E. Merzbacher, Quantum Mechanics (Wiley, New York, 1967).
18. J. L. Beeby and S. F. Edwards, Proc. R. Soc. A274, 395 (1963).
19. J. L. Beeby, Proc. R. Soc. A, 279, 82 (1964); Proc. R. Soc. A 302, 113 (1967).
20. S. Y. Tong and L. L. Kesmodel, Phys. Rev. B 8, 3753 (1973).

References contd.

21. S. Y. Tong and T. N. Rhodin, Phys. Rev. Lett. 26, 711 (1971).

22. R. H. Tait, S. Y. Tong, and T. N. Rhodin, Phys. Rev. Lett. 28, 553 (1972).

23. S. Y. Tong, T. N. Rhodin, and R. H. Tait, Phys. Rev. B 8, 421 (1973); Phys. Rev. B 8, 430 (1973).

24. J. B. Pendry, Phys. Rev. Lett. 27, 856 (1971).

25. M. G. Lagally, T. C. Ngoc, and M. B. Webb, Phys. Rev. Lett. 26, 1557 (1971); J. Vac. Sci. Technol. 9, 645 (1972).

26. T. C. Ngoc, M. G. Lagally and M. B. Webb, Surface Sci. 35, 117 (1973).

27. T. A. Clarke, R. Mason, and M. Tescari, Surface Sci. 30, 553 (1972); Proc. R. Soc. Lond. A 331, 321 (1972); Surface Sci. 40, 1 (1973).

28. J. C. Buchholz and M. G. Lagally, Surface Sci. 41, 248 (1974).

29. C. B. Duke and D. L. Smith, Phys. Rev. B 5, 4730 (1972).

30. J. B. Pendry, J. Phys. C 5, 2567 (1972).

31. G. E. Laramore and C. B. Duke, Phys. Rev. B 5, 267 (1972).

32. D. W. Jepsen, P. M. Marcus, and F. Jona, Phys. Rev. B 6, 3684 (1972).

33. M. R. Martin and G. A. Somorjai, Phys. Rev. B 7, 3607 (1973).

34. G. E. Laramore, Phys. Rev. B,(to be published).

35. J. E. Demuth, P. M. Marcus, and D. W. Jepsen, (to be published).

36. G. E. Laramore, Phys. Rev. B 8, 515 (1973).

37. D. W. Jepsen, P. M. Marcus, and F. Jona, Phys. Rev. B,(to be published).

38. S. Andersson and J. B. Pendry, J. Phys. C 5 L41 (1972).

39. F. Forstmann, W. Berndt, and P. Büttner, Phys. Rev. Lett. 30, 17 (1973).

40. J. E. Demuth, D. W. Jepsen, and P. M. Marcus, Phys. Rev. Lett. 31, 540 (1973); J. Phys. C 6 L 307 (1973).

References contd.

41. S. Andersson, B. Kasemo, J. B. Pendry, and M. A. Van Hove, Phys. Rev. Lett. 31, 595 (1973).

42. C. B. Duke, N. O. Lipari, and G. E. Laramore, Nuovo Cimento, (to be published).

43. C. B. Duke, N. O. Lipari, G. E. Laramore, and J. B. Theeten, Solid State Comm. 13, 579 (1973).

44. A. Ignatiev, F. Jona, D. W. Jepsen, and P. M. Marcus, Surface Sci. 40, 439 (1973).

45. F. Jona, IBM J. Res. Dev. 14, 4 (1970).

46. M. G. Lagally, T. C. Ngoc and M. B. Webb, J. Vac. Sci. Tech. 9, 645 (1972). J. E. Demuth, S. Y. Tong, and T. N. Rhodin, J. Vac Sci. Tech. 9, 639 (1972).

47. M. G. Lagally, Zeit. Naturforschung 25, 1567 (1970).

48. S. Andersson, Surf. Sci. 18, 325 (1969); R. J. Reid, Surf. Sci. 29, 603(1972).

49. E. G. McRae and G. W. Caldwell, Surf. Sci. 2, 509 (1967).

50. G. E. Laramore and A. C. Switendick, Phys. Rev. B 7, 3615 (1973).

51. T. E. Gallon, I. G. Higginbothom, M. Prutton and H. Tokutaka, Surf. Sci 21, 224 (1970).

52. G. C. Benson, J. Chem. Phys. 35, 2113 (1961).

53. C. E. Holcombe, Jr., G. L. Powell and R. E. Clausing, Surf. Sci. 30, 561 (1972).

54. W. R. Bottoms, (Private communication).

55. G. A. Somorjai, Principles of Surface Chemistry (Prentice Hall, New York, 1972).

References contd.

56. D. L. Heron and D. Haneman: Surface Sci., 21, 12 (1970).

57. J. J. Lander and J. Morrison: J. Chem. Phys., 33, 729 (1962).

58. J. B. Marsh and H. E. Farnsworth: Surface Sci., 1, 3 (1964).

59. A. E. Morgan and G. A. Somorjai: Surface Sci., 12, 405 (1968).

60. P. W. Palmberg and T. N. Rhodin: Phys. Rev., 161, 586 (1967).

61. J. T. Grant: Surface Sci., 18, 228 (1969).

62. F. Jona: Surface Sci., 8, 57 (1967).

63. S. Andersson, I. Marklund, and D. Andersson: in The Structure and Chemistry of Solid Surfaces, G. A. Somorjai, ed. John Wiley & Sons, Inc., New York, 1969.

64. A. U. MacRae and G. W. Gobeli: J. Appl. Phys., 35, 1629 (1964).

65. B. D. Campbell, G. A. Haque, and H. E. Farnsworth: in The Structure and Chemistry of Solid Surfaces, G. A. Somorjai, ed. John Wiley & Sons, Inc., New York, 1969.

66. M. F. Chung and H. E. Farnsworth, Surface Sci. 22, 93 (1970).

67. L. Fiermans and J. Vennik, Surface Sci., 18, 317 (1969).

68. T. M. French and G. A. Somorjai, J. Phys. Chem, 74, 2459 (1970).

69. D. Aberdam and C. Gaubert, Surface Sci., 27, 571 (1971).

70. W. Mönch, Adv. in Solid State Physics 13, 241 (1973).

71. B. A. Joyce, Surf. Sci. 35, 1 (1973).

72. A. Taloni and D. Haneman, Surf. Sci. 10, 215 (1968).

73. S. E. Trullinger and S. L. Cummingham, Phys. Rev. Lett. 30, 913 (1973).

74. F. J. Szalkowski and G. A. Somorjai, J. Chem. Phys. 56, 6097 (1972).

75. T. W. Haas, Surface Sci. 5, 345 (1966).

76. W. P. Ellis and R. L. Schwoebel, Surface Sci. 11, 82 (1968).

77. J. Perdereau and G. E. Rhead, Surf. Sci. 24, 555 (1971).

References contd.

78. M. Henzler, Surface Sci. 19, 159 (1970).

79. B. Lang, R. W. Joyner, and G. A. Somorjai, Surface Sci. 30, 440 (1972).

80. M. Henzler, Surface Sci. 22, 12 (1970).

81. B. D. Campbell and W. P. Ellis, Surface Sci. 10, 118 (1968).

82. J. E. Houston and R. L. Park, Surface Sci. 26, 269 (1971).

83. B. Lang, R. W. Joyner and G. A. Somorjai, Surf. Sci. 30, 454 (1972).

84. S. L. Bernasek, W. J. Siekhaus, and G. A. Somorjai, Phys. Rev. Lett. 30, 1202 (1973).

85. J. L. Gland and G. A. Somorjai, Surface Sci. 38, 157 (1973).

86. K. Baron, D. W. Blakely and G. A. Somorjai, Surface Sci. 41, 45 (1974).

87. B. Lang, R. W. Joyner and G. A. Somorjai, J. Catalysis 27, 405 (1972).

88. G. A. Somorjai and H. H. Farrell, Advan. Chem. Phys. 20, 215 (1971).

89. G. A. Somorjai, Surface Sci. 34, 156 (1973).

90. G. A. Somorjai and F. J. Szalkowski, J. Chem. Phys. 54, 389 (1971).

91. J. J. Lander and J. Morrison, Surface Sci. 6, 1 (1967).

92. P. W. Palmberg, Surface Sci. 25, 598 (1971).

93. M. A. Chesters and J. Pritchard, Surface Sci. 28, 460 (1971).

94. A. Ignatiev, A. V. Jones, and T. N. Rhodin, Surface Sci. 30, 573 (1972).

95. J. M. Dickey, H. H. Farrell, and M. Strongin, Surface Sci. 23, 448 (1970).

96. J. L. Gland and G. A. Somorjai, Surface Sci., 41, 387 (1974).

97. J. L. Gland, K. Baron, and G. A. Somorjai, Surface Sci., (to be published).

98. J. E. Demuth, Ph.D. dissertation (Cornell University, Ithaca, New York, 1973).

99. J. E. Demuth and T. N. Rhodin, (to be published).

100. K. Baron, R. B. Moyes, and R. C. Squire, Proc. 5th Intern. Congr. on Catalysis, Palm Beach, Florida, August, 1972.

Bibliography for Tables II, III, and IV

1. K. Muller, Zeits. Naturforschung, 20A, 153 (1965).
2. A. U. MacRae, Surface Sci. 1, 319 (1964).
3. L. H. Germer, E. J. Schneiber and C. D. Hartman, Phil. Mag. 5, 222 (1960).
4. R. L. Park and H. E. Farnsworth, Appl. Phys. Letters 3, 167 (1963).
5. T. Edmonds and R. C. Pitkethly, Surface Sci. 15, 137 (1969).
6. A. U. MacRae, Science 139, 379 (1963).
7. G. Ertl, Surface Sci. 6, 208 (1967).
8. N. Takahashi et al., C. R. Acad. Sci. 269 B, 618 (1969).
9. G. W. Simmons, D. F. Mitchell and K. R. Lawless, Surface Sci. 8, 130 (1967).
10. C. W. Tucker, Jr., Surface Sci. 2, 516 (1964).
11. C. W. Tucker, Jr., J. Appl. Phys. 35, 1897 (1964).
12. J. T. Grant and T. W. Haas, Surface Sci. 21, 76 (1970).
13. W. P. Ellis, J. Chem. Phys. 48, 5695 (1968).
14. J. Ferrante and G. C. Barton, NASA Tech. Note D-4735, 1968.
15. N. J. Taylor, Surface Sci. 2, 544 (1964).
16. J. B. Marsh and H. E. Farnsworth, Surface Sci. 1, 3 (1964).
17. R. E. Schlier and H. E. Farnsworth, J. Chem. Phys. 30, 917 (1959).
18. H. E. Farnsworth, R. E. Schlier, T. H. George and R. M. Buerger, J. Appl. Phys. 29, 1150 (1958).
19. J. J. Lander and J. Morrison, J. Appl. Phys. 34, 1411 (1963).
20. J. J. Lander and J. Morrison, J. Appl. Phys. 33, 2089 (1962).
21. G. Rovida et al., Surface Sci. 14, 93 (1969).

22. R. O. Adams, The Structure and Chemistry of Solid Surfaces, ed. G. A. Somorjai, John Wiley and Sons, Inc., New York, 1969.

23. H. E. Farnsworth and D. M. Zehner, Surface Sci. 17, 7 (1969).

24. G. J. Dooley and T. W. Haas, Surface Sci. 19, 1 (1970).

25. B. D. Campbell, C. A. Haque and H. E. Farnsworth, The Structure and Chemistry of Solid Surfaces, ed. G. A. Somorjai, John Wiley and Sons, Inc., New York, 1969.

26. G. Ertl, Surface Sci. 7, 309 (1967).

27. T. Edmonds and R. C. Pitkethly, Surface Sci. 17, 450 (1969).

28. A. E. Morgan and G. A. Somorjai, J. Chem. Phys. 51, 3309 (1969).

29. J. C. Bertolini and G. Dalmai-Imelik, Coll. Intern. CNRS, Paris, 7-11 July 1969.

30. J. J. Lander and J. Morrison, Surface Sci. 4, 241 (1966).

31. L. H. Germer and A. U. MacRae, J. Chem. Phys. 36, 1555 (1962).

32. A. J. van Bommel and F. Meyer, Surface Sci. 8, 381 (1967).

33. J. J. Lander and J. Morrison, J. Chem. Phys. 37, 729 (1962).

34. R. Heckingbottom, The Structure and Chemistry of Solid Surfaces, ed. G. A. Somorjai, John Wiley and Sons, Inc., New York 1969.

35. J. L. Domange and J. Oudar, Surface Sci. 11, 124 (1968).

36. M. Perdereau and J. Oudar, Surface Sci. 20, 80 (1970).

37. A. J. van Bommel and F. Meyer, Surface Sci. 6, 391 (1967).

38. J. V. Florio and W. D. Robertson, Surface Sci. 18, 398 (1969).

39. J. C. Bertolini and G. Dalmai-Imelik, Rapport Inst. de Rech. sur la Catalyse, Villeurbanne, 1969.

40. D. L. Smith and R. P. Merrill, J. Chem. Phys. 52, 5861 (1970).

41. M. Boudart and D. F. Ollis, The Structure and Chemistry of Solid Surfaces, ed. G. A. Somorjai, John Wiley and Sons, Inc., New York, 1969.

42. F. Jona, J. Phys. Chem. Solids 28, 2155 (1967).

43. S. M. Bedair, F. Hoffmann and H. P. Smith, Jr., J. Appl. Phys. 39, 4026 (1968).

44. H. H. Farrell, Ph.D. Dissertation, University of California, Berkeley, 1969.

45. L. K. Jordan and E. J. Scheibner, Surface Sci. 10, 373 (1968).

46. L. Trepte, C. Menzel-Kopp and E. Mensel, Surface Sci. 8, 223 (1967).

47. R. N. Lee and H. E. Farnsworth, Surface Sci. 3, 461 (1965).

48. J. T. Grant, Surface Sci. 18, 228 (1969).

49. R. E. Schlier and H. E. Farnsworth, J. Appl. Phys. 25, 1333 (1954).

50. H. E. Farnsworth and J. Tuul, J. Phys. Chem. Solids 9, 48 (1958).

51. J. W. May and L. H. Germer, Surface Sci. 11, 443 (1968).

52. R. E. Schlier and H. E. Farnsworth, Advances Catalysis 9, 434 (1957).

53. L. H. Germer and C. D. Hartman, J. Appl. Phys. 31, 2085 (1960).

54. H. E. Farnsworth and H. H. Madden, Jr., J. Appl. Phys. 32, 1933 (1961).

55. R. L. Park and H. E. Farnsworth, J. Chem. Phys. 43, 2351 (1965).

56. L. H. Germer, Advances Catalysis 13, 191 (1962).

57. L. H. Germer, R. Stern and A. U. MacRae, Metal Surfaces ASM, Metals Park, Ohio, 1963, p. 287.

58. C. W. Tucker, Jr., J. Appl. Phys. 37, 3013 (1966).

59. C. A. Haque and H. E. Farnsworth, Surface Sci. 1, 378 (1964).

60. A. J. Pignocco and G. E. Pellissier, J. Electrochem. Soc. 112, 1188 (1965).

61. H. K. A. Kann and S. Feuerstein, J. Chem. Phys. 50, 3618 (1969).

62. K. Hayek and H. E. Farnsworth, Surface Sci. 10, 429 (1968).

63. H. E. Farnsworth and K. Hayek, Suppl. Nuovo Cimento, 5, 2 (1967).

64. G. J. Dooley and T. W. Haas, J. Chem. Phys. 52, 461 (1970).

65. K. K. Vijai and P. F. Packman, J. Chem. Phys. 50, 1343 (1969).

66. P. J. Estrup, The Structure and Chemistry of Solid Surfaces, ed. G. A. Somorjai, John Wiley and Sons, Inc., New York, 1969.

67. J. Anderson and W. E. Danforth, J. Franklin Inst. 279, 160 (1965).

68. M. Onchi and H. E. Farnsworth, Surface Sci. 11, 203 (1968).

69. R. A. Armstrong, The Structure and Chemistry of Solid Surfaces, ed. G. A. Somorjai, John Wiley and Sons, Inc., New York, 1969.

70. J. C. Tracy and P. W. Palmberg, J. Chem. Phys. 51, 4852 (1969).

71. R. L. Park and H. H. Madden, Surface Sci. 11, 188 (1968).

72. A. E. Morgan and G. A. Somorjai, Surface Sci. 12, 405 (1968).

73. C. Burggraf and A. Mosser, C.R. Acad. Sci. 268 B, 1167 (1969).

74. A. E. Morgan and G. A. Somorjai, Trans. Am. Cryst. Assoc. 4, 59 (1968).

75. J. Anderson and P. J. Estrup, J. Chem. Phys. 46, 563 (1967).

76. M. Onchi and H. E. Farnsworth, Surface Sci. 13, 425 (1969).

77. G. J. Dooley and T. W. Haas, J. Chem. Phys. 52, 993 (1970).

78. P. W. Tamm and L. D. Schmidt, J. Chem. Phys. 51, 5352 (1969).

79. P. J. Estrup and J. Anderson, J. Chem. Phys. 45, 2254 (1966).

80. H. H. Madden and H. E. Farnsworth, J. Chem. Phys. 34, 1186 (1961).

81. J. W. May and L. H. Germer, The Structure and Chemistry of Surfaces, ed. G. A. Somorjai, John Wiley and Sons, Inc., New York, 1969.

82. P. J. Estrup and J. Anderson, J. Chem. Phys., 46, 567 (1967).

83. T. L. Park and H. E. Farnsworth, J. Appl. Phys. 35, 2220 (1964).

84. P. J. Estrup and J. Anderson, J. Chem. Phys. 49, 523 (1968).

85. E. Margot et al., C. R. Acad. Sci. 270 C, 1261 (1970).

86. N. W. Tideswell and J. M. Ballingal, J. Vac. Sci. Techn. 7, 496 (1970).

87. F. Portele, Zeits. Naturforschung 24 A, 1268 (1969).

88. G. Dalmai-Imelik and J. C. Bertolini, C.R. Acad. Sci. 270, 1079 (1970).

89. L. H. Germer and A. U. MacRae, J. Appl. Phys. 33, 2923 (1962).

90. L. H. Germer, A. U. MacRae and A. Robert, Welch Foundation Research, Bull. No. 11, 1961, p. 5.

91. R. L. Park and H. E. Farnsworth, J. Chem. Phys. 40, 2354 (1964).

92. L. H. Germer, J. W. May and R. J. Szostak, Surface Sci. 7, 430 (1967).

93. J. W. May, L. H. Germer and C. C. Chang, J. Chem. Phys. 45, 2383 (1966).

94. A. G. Jackson and M. P. Hooker, Surface Sci. 6, 297 (1967).

95. G. Ertl and P. Rau, Surface Sci. 15, 443 (1969).

96. C. W. Tucker, Jr., J. Appl. Phys. 38, 2696 (1967).

97. C. W. Tucker, Jr., J. Appl. Phys. 37, 4147 (1966).

98. A. J. Pignocco and G. E. Pellisier, Surface Sci. 7, 261 (1967).

99. K. Moliere and F. Portele, The Structure and Chemistry of Solid Surfaces, ed. G. A. Somorjai, John Wiley and Sons, Inc., N. Y. 1969.

100. T. W. Haas and A. G. Jackson, J. Chem. Phys. 44, 2921 (1966).

101. T. W. Haas, A. G. Jackson and M. P. Hooker, J. Chem. Phys. 46, 3025, (1967).

102. T. W. Haas, The Structure and Chemistry of Solid Surfaces, ed. G. A. Somorjai, John Wiley and Sons, Inc., N. Y. 1969.

103. L. H. Germer, Physics Today, July 1964, p. 19.

104. L. H. Germer and J. W. May, Surface Sci. 4, 452 (1966).

105. G. J. Dooley and T. W. Haas, J. Vac. Sci. Techn. 7, 49 (1970).

106. C. C. Chang and L. H. Germer, Surface Sci. 8, 115 (1967).

107. T. C. Tracy and J. M. Blakeley, The Structure and Chemistry of Solid Surfaces, ed. G. A. Somorjai, John Wiley and Sons, Inc., N. Y., 1969.

108. C. C. Chang, J. Electrochem. Soc. 115, 354 (1968).

109. J. W. May and L. H. Germer, J. Chem. Phys. 44, 2895 (1966).

110. L. H. Germer and A. U. MacRae, Proc. Natl. Acad. Sci. U.S. 48, 997 (1962).

111. T. W. Haas, J. Appl. Phys. 39, 5854 (1968).

112. D. L. Adams et al., Surface Sci. 22, 45 (1970).

113. J. W. May, R. J. Szostak and L. H. Germer, Surface Sci. 15, 37 (1969).

114. D. H. Buckley, NASA Techn. Note D-5689, 1970.

115. I. Marklund, S. Andersson and J. Martinsson, Arkiv for Fysik 37, 127 (1968).

116. P. Legare and G. Marie, J. Chim. Phys. Physsichim. Biol. 68 (7-8), 1206 (1971).

117. G. Marie, J. R. Anderson, and B. B. Johnson, Proc. Roy. Soc. Lond. A, 320, 227 (1970).

118. T. Edmonds, J. J. McCarrol and R. C. Pitkethly, J. Vac. Sci. Tech. 8 (1), 68 (1971).

119. K. Okado, T. Halsushika, H. Tomita, S. Motov and N. Takalashi, Shinku 13 (11), 371 (1970).

120. B. Lang, R. W. Joyner, and G. A. Somorjai, Surf. Sci. 30, 454 (1972).

121. M. Henzler, and J. Töpler, Surf. Sci. 40, 388 (1973).

122. H. Van Hove, R. Leysen, Phys. Status Solidi A, 9 (1), 361 (1972).

123. S. M. Bedair and H. P. Smith, Jr., J. Appl. Phys. 42, 3616 (1971).

124. J. T. Grant, Surface Sci. 25, 451 (1971).

125. R. W. Joyner, C. S. McKee and M. W. Roberts, Surface Sci. 26, 303 (1971).

126. J. C. Tracy, J. Chem. Phys. 56 (6), 2748 (1971).

127. M. A. Chesters and J. Pritchard, Surface Sci. 28, 460 (1971).

128. R. W. Joyner, C. S. McKee and M. W. Roberts, Surface Sci. 27, 279 (1971).

129. J. C. Tracy, J. Chem. Phys. 56 (6), 2736 (1971).

130. D. Tabor and J. M. Wilson, J. Cryst. Growth 9, 60 (1971).

131. D. L. Adams and L. H. Germer, Surface Sci. 27, 21 (1971).

132. J. Perdereau and G. E. Rhead, Surface Sci. 24, 555 (1971).

133. P. W. Palmberg, Surface Sci. 25, 104 (1971).

134. G. Erth and J. Kuppers, Surface Sci. 24, 104 (1971).

135. R. Heckingbottom and P. R. Wood, Surface Sci. 23, 437 (1970).

136. K. J. Matysik, Surface Sci. 29, 324 (1972).

137. G. E. Becker and H. D. Hagstrum, Surface Sci. 30, 505 (1972).

138. D. L. Adams and L. H. Germer, Surface Sci. 32, 205 (1972).

139. H. P. Bonzel and R. Ku, Surface Sci. 33, 91 (1972).

140. P. Michel and Ch. Jardin, Surface Sci. 36, 478 (1973).

141. A. Melmed and J. J. Carroll, J. Vac. Sci. Technol., 10, 164 (1973).

142. H. D. Hagstrum and G. E. Becker, Phys. Rev. Lett. 22, 1054 (1969); J. Chem. Phys. 54, 1015 (1971).

143. W. H. Weinberg and R. P. Merrill, Surface Sci. 32, 317 (1972).

144. P. B. Sewell, D. F. Mitchell and M. Cohen, Surface Sci. 33, 535 (1972).

145. F. Forstmann, W. Berndt, and P. Büttner, Phys. Rev. Lett. 30, 17 (1973).

Table I

Angles of Cut, Miller Indices, and Designation of the Stepped Platinum Surfaces

Angle of Cut	Miller Index	Designation
6.2° from (111)	(533)	Pt(S)-[9(111)x(100)]
9.5° from (111)	(755)	Pt(S)-[6(111)x(100)]
14.5° from (111)	(544)	Pt(S)-[4(111)x(100)]
9.5° from (111) rotated 20°	(976)	Pt(S)-[7(111)x(310)]

Table II. Surface Structures on Substrates with Sixfold Rotational Symmetry

Surface	Adsorbed Gas	Surface Structure	Reference
Ag(111)	O_2	(2 × 2)-O	1
		$(\sqrt{3} \times \sqrt{3})$R 30°-O	1
	I_2	$(\sqrt{3} \times \sqrt{3})$R 30°-I	145
	CO + O_2	(2 × $\sqrt{3}$)-(CO + O_2)	27
Al(111)	O_2	(4 × 4)-O	123
Be(0001)	O_2	Disordered	22
	CO	Disordered	22
	H_2	Not adsorbed	22
	N_2	Not adsorbed	22
C(diamond)(111)	O_2	Adsorbed	16
	H_2	(1 × 1)-H	30
	P	$(\sqrt{3} \times \sqrt{3})$R 30°-P	30
CdS(0001)	O_2	Disordered	25
Cu(111)	O_2	Disordered	7
		(7 × 7)-O	7,8
		$(\sqrt{3} \times \sqrt{3})$R30°-O	7,8
		(2 × 2)-O	115,7,8
		(3 × 3)-O	8
		(11 × 5)R 5°-O	9
		(2 × 2)R 30°-O	115,119
	CO	Not adsorbed	26
	H_2	Not adsorbed	7
	H_2S	$(\sqrt{3} \times \sqrt{3})$R 30°-S	35
		Adsorbed	35
	C_2H_4	Not adsorbed	26
Ge(111)	O_2	Disordered	17,18
		(1 × 1)	19,21
	P	(1 × 1)-P	19
	H_2S	(2 × 2)-S	37
	H_2Se	(2 × 2)-Se	37
	I_2	(1 × 1)-I	19
	H_2O	(1 × 1)	121
Ir(111)	O_2	(2 × 2)-O	124
	CO	$(\sqrt{3} \times \sqrt{3})$-CO	124
Mo(111)	O_2	To (211) facets	14
Ni(111)	O_2	(2 × 2)-O	2,3,4,116
		$(\sqrt{3} \times \sqrt{3})$R 30°-O	2,5
		NiO(111)	4,6,116
		$(\sqrt{3} \times \sqrt{21})$-O	116
	CO	(2 × 2)-CO	3
		$(\sqrt{3} \times \sqrt{3})$R 30°-O	5
		(2 × $\sqrt{3}$)-CO	5
		$(\sqrt{39} \times \sqrt{39})$-C	5,27
	CO_2	(2 × 2)-CO_2	5
		$(\sqrt{3} \times \sqrt{3})$R 30°-O	5
		(2 × $\sqrt{3}$)-CO_2	5
		$(\sqrt{39} \times \sqrt{39})$-C	5,27
	H_2	(1 × 1)-H	3
		(2 × 2)-H	29

Table II. Surface Structures on Substrates with Sixfold Rotational Symmetry (Continued)

Surface	Adsorbed Gas	Surface Structure	Reference
	N_2	Not adsorbed	31
	H_2S	(2 × 2)-S	36,118
		$(\sqrt{3} \times \sqrt{3})R\ 30°$-S	36,118
		(5 × 5)-S	36
		Adsorbed	36
	H_2Se	(2 × 2)-Se	137
		$(\sqrt{3} \times \sqrt{3})R\ 30°$-Se	137
	CH_4	(2 × 2)-CH_4	117
		(2 × $\sqrt{3}$)-CH_4	117
	C_2H_4	(2 × 2)-C_2H_4	29,39
		Adsorbed	29
	C_2H_6	(2 × 2)-C_2H_6	39,117
		$(\sqrt{7} \times \sqrt{7})R\ 19°$-C	29
		(2 × $\sqrt{3}$)-C_2H_5	117
Pt(111)	O_2	(2 × 2)-O	10,11
		Not adsorbed	120
	CO	c(4 × 2)-CO	28,120
		(2 × 2)-CO	120
	H_2	Not adsorbed	120
	$H_2 + O_2$	$(\sqrt{3} \times \sqrt{3})R\ 30°$ -	11
	C_2H_4	(2 × 1)-C_2H_4	28
		(2 × 2)-C_2H_4	40
	C_2H_2	(2 × 1)-C_2H_2	28
Pt(S)-[6(111)×(100)]	O_2	2(1d)-O	120
	CO	Disordered	120
	H_2	2(1d)-H	120
	C_2H_4	(2 × 2)-C_2H_4	120
Pt(S)-[9(111)×(111)]	O_2	Not adsorbed	120
	CO	Disordered	120
	H_2	(2 × 2)-H	120
	C_2H_4	Dirordered	120
	$H_2 + CO_2$	$(\sqrt{3} \times \sqrt{3})R\ 30°$-($H_2$ + CO_2)	120
Re(0001)	O_2	(2 × 2)-O	23,24
	CO	Not adsorbed	24
		(2 × 2)-CO	23
	H_2	Not adsorbed	24
	H_2	Not adsorbed	24
Rh(111)	O_2	(2 × 2)-O	12
	CO	(2 × 2)-CO	12
Ru(0001)	O_2	(2 × 2)-O	12
	CO	$(\sqrt{3} \times \sqrt{3})R\ 30°$-CO	12
		(2 × 2)-CO	12
	CO_2	$(\sqrt{3} \times \sqrt{3})R\ 30°$-$CO_2$	12
		(2 × 2)-CO_2	12
Si(111)	O_2	Disordered	17,20,21
	N_2	(8 × 8)-N	34
	P	(6$\sqrt{3}$ × 6$\sqrt{3}$)-P	32,33
		(1 × 1)-P	32
		(2$\sqrt{3}$ × 2$\sqrt{3}$)-P	32
		(4 × 4)-P	33
	Cl_2	Disordered	38
		(7 × 7)-Cl	38
		(1 × 1)-Cl	38
	I_2	(1 × 1)-I	33
Ti(0001)	O_2	(1 × 1)-O	18
	CO	(1 × 1)-CO	18
UO_2(111)	O_2	(3 × 3)-O	13
		(2$\sqrt{3}$ × 2$\sqrt{3}$)R 30°-O	13
W(111)	O_2	To (211) facets	15
	CH_4	(6 × 6)-C	41
Zn(0001)	O_2	(1 × 1)-O	122
Zn(000$\bar{1}$)	O_2	($\sqrt{3}$ × $\sqrt{3}$)-O	122

Table III. Surface Structures on Substrates with Fourfold Rotational Symmetry

Surface	Adsorbed Gas	Surface Structure	Reference
Al(100)	O_2	Disordered	42,43,44
C(diamond)(100)	O_2	Disordered	16
		Adsorbed	16
Cr(100)	O_2	(2 × 2)-O	59
		c(2 × 2)-O	140
	CO	(2 × 2)-CO	59
	N_2	(2 × 2)-N	59
Cu(100)	O_2	(1 × 1)-O	9,45
		(2 × 1)-O	9,45,46
		(2 × 4)R 45°-O	7,47
		Adsorbed	7,47
		(2 × 3)-O	119
		c(4 × 4)-O	119
	CO	(2 × 2)-C	26,125
		c(2 × 2)-CO	125,126
		Compressed c(2 × 2)-CO	126,127
	N_2	(1 × 1)-N	49
		c(2 × 2)-N	47,132
	H_2S	(2 × 2)-S	35
		Adsorbed	35
		(2 × 1)-S	128
	C_2H_4	(2 × 2)-C_2H_4	26
Cu(S)-[3(100)×(100)]	CO	Not adsorbed	132
	N_2	(1 × 2)-N	132
	CH_4	Not adsorbed	132
	C_2H_4	Not adsorbed	132
Cu(S)-[4(100)×(100)]	O_2	(1 × 1)-O	132
	CO	Not adsorbed	132
	N_2	(1 × 3)-N	132
	CH_4	Not adsorbed	132
	C_2H_4	Not adsorbed	132
Cu(S)-[4(100)×(111)]	H_2S	S(1d)-S	35
Fe(100)	O_2	c(2 × 2)-O	60
		FeO(100)	60
		(1 × 1)-O	144
	H_2S	c(2 × 2)-S	85
		c(22 × 2)R 45°-S	85
		c(18 × 2)R 45°-S	85
		c(14 × 2)R 45°-S	85
		c(10 × 2)R 45°-S	85
Ge(100)	O_2	Disordered	17,18
	I_2	(3 × 3)-I	19
Ir(100)	O_2	(2 × 1)-O	48
		(5 × 1)-O	48
	CO	c(2 × 2)-CO	48
	CO_2	c(2 × 2)-CO_2	48
		(7 × 20)-CO_2	48
Mo(100)	O_2	Disordered	61,62
		c(2 × 2)-O	61,62,63,64
		($\sqrt{5}$ × $\sqrt{5}$)R 26°-O	61,62
		(2 × 2)-O	61
		c(4 × 4)-O	62
	CO	Disordered	62
		(1 × 1)-CO	62,64
		c(2 × 2)-CO	64
		(4 × 1)-CO	64
	N_2	c(4 × 2)-N	77
		(1 × 1)-N	77
	N_2	(1 × 1)-N	62
	H_2S	(1 × 1)-S	130
		($\sqrt{5}$ × $\sqrt{5}$)-S	130
		c(2 × 2)-S	130

Table III. Surface Structures on Substrates with Fourfold Rotational Symmetry (Continued)

Surface	Adsorbed Gas	Surface Structure	Reference
Ni(100)	O_2	(2 × 2)-O	2,49,50,51
		c(2 × 2)-O	2,52-57,6
		NiO(100)	6
	CO	c(2 × 2)-CO	54,55,68,129
		(2 × 2)-CO	69
		Hexagonal overlayer in [$\bar{1}00$]	129
	CO_2	Decomposition to (2 × 2)-O + c(2 × 2)-CO	76
	N_2	Not adsorbed	80,81
	H_2S	(2 × 2)-S	36,118
		c(2 × 2)-S	36,118
	H_2Se	c(2 × 2)-Se	142
	SO_2	c(2 × 2)-SO_2	86
		(2 × 2)-SO_2	86
	CH_4	c(2 × 2)-CH_4	117
		(2 × 2)-CH_4	117
	C_2H_4	c(2 × 2)-C_2H_4	88
		($\sqrt{7}$ × $\sqrt{7}$)R 19°-C	88
	C_2H_6	c(2 × 2)-C_2H_6	117
		(2 × 2)	117
Pd(100)	CO	Disordered	70
		c(4 × 2)-CO	70
		(2 × 4)R 45°-CO	71
Pt(100)	O_2	Not adsorbed	120
	CO	c(4 × 2)-CO	28,72,73,120
		($3\sqrt{2}$ × $\sqrt{2}$)R 45°-CO	28,72,73
		($\sqrt{2}$ × $\sqrt{5}$)R 45°-CO	72,75
		(2 × 4)-CO	10
		(1 × 3)-CO	10
		(1 × 1)-CO	120
	H_2	(2 × 2)-H	72,74
	CO + H_2	c(2 × 2)-(CO + H_2)	72,74
	C_2H_4	c(2 × 2)-C_2H_4	28,72
	C_2H_2	c(2 × 2)-C_2H_2	28,72
Rh(100)	O_2	c(2 × 8)-O	58
	CO	(4 × 1)-CO	58
Si(100)	O_2	(1 × 1)-O	17,18,20
		To (111) facets	17,18,20
V(100)	O_2	(1 × 1)-O	65
		(2 × 2)-O	65
	N_2	Disordered	65
W(100)	O_2	(4 × 1)-O	66
		(2 × 1)-O	66,67
		To (110) facets	66
	CO	Disordered	75
		c(2 × 2)-CO	66,75
	H_2	c(2 × 2)-H	66,78,79
		(2 × 5)-H	79
		(4 × 1)-H	79
	N_2	c(2 × 2)-N	66,82,131
	NH_3	Disordered	84
		c(2 × 2)-NH_2	84
		(1 × 1)-NH_2	84
	N_2O	(1 × 1)-N_2O	143
		(4 × 1)-N_2O	143
	CO + N_2	(4 × 1)-(CO + N_2)	82
	CH_4	(5 × 1)-C	41

Table IV. Surface Structures on Substrates with Twofold Rotational Symmetry.

Surface	Adsorbed Gas	Surface Structure	Reference
Al(110)	O_2	(331) facets	123
		(111) facets	122
Cr(110)	O_2	(3 × 1)-O	140
		(100) facets	140
Cu(110)	O_2	(2 × 1)-O	7,8,9,45,46
		c(6 × 2)-O	8,9,45,46
		(5 × 3)-O	8,115
	CO	Ord. 1D	26
		(2 × 3)-CO	26
	H_2	Not adsorbed	7
	H_2O	Disordered	26
	H_2S	c(2 × 3)-S	35
		Adsorbed	35
	C_2H_4	Ord. 1D	26
Cu/Ni(110)	O_2	(2 × 1)-O	134
-(55% Cu bulk)	CO	(2 × 1)-CO	134
		(2 × 2)-CO	134
	H_2S	c(2 × 2)-S	134
Fe(110)	O_2	c(2 × 2)-O	87,98,99
		c(3 × 1)-O	87,98,99
		(2 × 8)-O	98
		FeO(111)	87,98,99
		(2 × 1)-O	141
	H_2S	(2 × 4)-S	114
		(1 × 2)-S	114
Ge(110)	O_2	Disordered	17,18
		(1 × 1)	17,18
Mo(110)	O_2	(2 × 2)-O	62,63,100
		(2 × 1)-O	62,63,100
		(1 × 1)-O	62,63
	CO	(1 × 1)-CO	62,100
		c(2 × 2)-CO	94
	CO_2	Disordered	94
	H_2	Adsorbed	100
	H_2	(1 × 1)-H	62
Mo(211)	O_2	(2 × 1)-O	105
		(1 × 2)-O	105
		(1 × 3)-O	105
		c(4 × 2)-O	105
	CO	Adsorbed	105
		Disordered	105
	H_2	(1 × 2)-H	105
	H_2	Not adsorbed	105
Nb(110)	O_2	(3 × 1)-O	101
		Oxide	101
	CO	Disordered	101
		Decomposition to (3 × 1)-O	101
	H_2	(1 × 1)-H	111
Ni(110)	O_2	(2 × 1)-O	2,3,51,57,89, 99,91,92,83
		(3 × 1)-O	2,51,89,91,92, 83,94
		(5 × 1)-O	2,89
		(9 × 4)-O	51
		NiO(100)	6,51,91,83
	CO	(1 × 1)-CO	2,94
	H_2	(1 × 2)-H	59,81,94,110
	H_2O	(2 × 1)-H_2O	110
	H_2S	c(2 × 2)-S	36
		(3 × 2)-S	36
	H_2Se	c(2 × 2)-Se	137
	CO + O_2	(3 × 1)-(CO + O_2)	91
	CH_4	(2 × 2)-CH_4	117
		(4 × 3)	117
		(4 × 5)	117

Table IV. Surface Structures on Substrates with Twofold Rotational Symmetry (Continued)

Surface	Adsorbed Gas	Surface Structure	Reference
	C_2H_6	(2 × 2)	117
Pd(110)	O_2	(1 × 3)-O	95
		(1 × 2)-O	95
		c(2 × 4)-O	95
		Adsorbed	95
	CO	(5 × 2)-CO	95
		(2 × 1)-CO	95
Pt(110)	O_2	(2 × 1)-O	11
		(4 × 2)-O	11
	CO	(1 × 1)-CO	139
Rh(110)	O_2	Disordered	96,97
		c(2 × 4)-O	96,97
		c(2 × 8)-O	96,97
		(2 × 2)-O	96,97
		(2 × 3)-O	96,97
		c(2 × 2)-O	96,97
		(1 × 2)-O	96,97
		(1 × 3)-O	96,97
Si(311)-(3 × 1)	C_2H_4	Disordered	135
		c(1 × 1)	135
		(2 × 1)	135
		(3 × 1)	135
	C_2H_2	Disordered	135
		c(1 × 1)	135
		(2 × 1)	135
		(3 × 1)	135
Ta(110)	O_2	(3 × 1)-O	101,102
		Oxide	101,102
	CO	Disordered	101,102
		Decomposition to (3 × 1)-O	101,102
	H_2	(1 × 1)-H	102
	N_2	Not adsorbed	101
Ta(211)	O_2	(3 × 1)-O	101,102
		Oxide	101,102
	CO	Disordered	101,102
		Decomposition (3 × 1)-O	102
	H_2	(1 × 1)-H	102
	N_2	Disordered	102
		To (311) facets	102
V(110)	O_2	(3 × 1)-O	101
	CO	Disordered	101
		Decomposition to (3 × 1)-O	101
W(110)	O_2	(2 × 1)-O	57,103
		c(2 × 2)-O	104
		(2 × 2)-O	104
		(1 × 1)-O	104
		c(14 × 7)-O	57,103,104
		c(21 × 7)-O	104
		c(48 × 16)-O	104
	CO	Disordered	109
		c(9 × 5)-CO	109
	CO + O_2	c(11 × 5)-(CO + O_2)	93
	C_2H_4	(15 × 3)R_1-C	41
		(15 × 12)R_1-C	41
	H_2	(2 × 1)-H	136

Table IV. Surface Structures on Substrates with Twofold Rotational Symmetry (Continued)

Surface	Adsorbed Gas	Surface Structure	Reference
W(211)	O_2	(2 × 1)-O	15,106,107,108
		(1 × 2)-O	15,106
		(1 × n)-O, n=1,2,3,4	106
		(1 × 1)	107
	CO	Disordered	108
		c(6 × 4)-CO	108
		(2 × 1)-CO	108
		c(2 × 4)-CO	108
		Adsorbed	108
	H_2	(1 × 1)-H	112
	NH_3	c(4 × 2)-NH_2	113
	CO + O_2	(1 × 1)-(CO + O_2)	108
		(1 × 2)-(CO + O_2)	108
W(210)	CO	(2 × 1)-CO	138
		(1 × 1)-CO	138
	N_2	(2 × 1)-N	131
W(310)	N_2	(2 × 1)-N	131
		c(2 × 2)-N	131

Table V

Work Function Changes and Structural Information for Adsorption of Organic Compounds on the Pt(111) and Pt(100)-(5×1) Surfaces

		Pt(111)			Pt(100)-(5×1)			
Adsorbate	Temp °C	Work Function Change		Adsorbate Diffraction Features or Surface Structure	Work Function Change		Substrate Structure after Adsorption	Adsorbate Diffraction Features or Surface Structures
		Press (Torr)	WFC (Volts)		Press (Torr)	WFC (Volts)		
Acetylene	20°	1×10^{-8}	- 1.5	(2×2)	4×10^{-7}	- 1.65	(1×1)	$(\sqrt{2}\times\sqrt{2})R45°$
	20°	1×10^{-8} (10 min)	- 1.65	disordered				
	150°	4×10^{-7}	- 1.8	disordered	4×10^{-7}	- 1.7	(1×1)	$(\sqrt{2}\times\sqrt{2})R45°$
Aniline	20°	1×10^{-8}	- 1.8	Streaks at 1/3 order diffuse (1/2 0) features	1×10^{-8}	- 1.75	(1×1)	disordered
Benzene	20°	4×10^{-7}	- 1.8	poorly ordered	3×10^{-7}	- 1.6	(1×1)	diffuse ring-like 1/2 order streak
	20°	4×10^{-7} (5 min)	- 1.4	$\begin{vmatrix} -2 & 2 \\ 4 & 4 \end{vmatrix}$				
	20°	4×10^{-7} (40 min)	- .7	$\begin{vmatrix} -2 & 2 \\ 5 & 5 \end{vmatrix}$	3×10^{-7} (2 hrs)	- 1.3	(1×1)	diffuse 1/2 order streak
Biphenyl	20°	2×10^{-9}	- 1.85	very poorly ordered	2×10^{-9}	- 1.8	(1×1)	disordered
n-Butylbenzene	20°	8×10^{-9}	- 1.5	disordered	8×10^{-9}	- 1.5	(1×1)	disordered
t-Butylbenzene	20°	5×10^{-8}	- 1.7	disordered	5×10^{-8}	- 1.75	(1×1)	disordered
Cyanobenzene	20°	1×10^{-8}	- 1.6	diffuse (1/3 0) features	1×10^{-8}	- 1.5	faint (5×1)	disordered
1,3-Cyclohexadiene	20°	2×10^{-8}	- 1.75	poorly ordered	2×10^{-9}	- 1.7	(1×1)	diffuse 1/2 order streak
	20°C	2×10^{-8} (1 hr)	- 1.3	$\begin{vmatrix} -2 & 2 \\ 4 & 4 \end{vmatrix}$	2×10^{-8} (1 hr)	- 1.6	(1×1)	diffuse 1/2 order streak
	20°C	3×10^{-7} (5 hrs)	- .8	$\begin{vmatrix} -2 & 2 \\ 5 & 5 \end{vmatrix}$	2×10^{-8} (5 hrs)	- 1.4	(1×1)	diffuse 1/2 order streak
Cyclohexane	20°	6×10^{-9}	- 1.2	(1×1) low background	6×10^{-9}	- .75	(5×1)	low background
	20°	4×10^{-7}	- .7	very poorly ordered	4×10^{-7}	- .4	(1×1)	diffuse streaked (2×1) pattern
	150°	4×10^{-7}	- 1.1	apparent (2×2)	4×10^{-7}	- 1.2	(1×1)	streaked (2×1) pattern
	300°	4×10^{-7}	- 1.4	disordered	4×10^{-7}	- 1.5	(1×1)	disordered
Cyclohexene	20°	6×10^{-7}	- 1.7	$\begin{vmatrix} 2 & 2 \\ 4 & -2 \end{vmatrix}$	6×10^{-7}	- 1.6	(1×1)	diffuse (1/2 0) features
	150°	6×10^{-7}	- 1.6	apparent (2×2)	6×10^{-7}	- 1.5	(1×1)	streaked (2×1) pattern
Cyclopentane	20°	7×10^{-9}	- .95	(1×1) low background	7×10^{-9}	- .4	(5×1)	low background
	20°	4×10^{-7}	- .7	disordered	4×10^{-7}	- .3	(1×1)	diffuse features at 1/2 order
Cyclopentene	20°	-	-	----	2×10^{-7}	- 1.4	(1×1)	diffuse streaked (1/2 0) features
2,6-Dimethyl-pyridine	20°	4×10^{-8}	- 1.6	diffuse 1/3.2, 2/3.2 order streaks	4×10^{-8}	- 1.5	faint (5×1)	disordered
3,5-Dimethyl-pyridine	20°	6×10^{-8}	- 2.3	diffuse 1/2 order streak	6×10^{-8}	- 2.2	(1×1)	disordered

Table V (continued)

Work Function Changes and Structural Information for Adsorption of Organic Compounds on the Pt(111) and Pt(100)-(5×1) Surfaces

		Pt(111)			Pt(100)-(5×1)			
Adsorbate	Temp °C	Work Function Change		Adsorbate Diffraction Features or Surface Structure	Work Function Change		Substrate Structure after Adsorption	Adsorbate Diffraction Features or Surface Structures
		Press (Torr)	WFC (Volts)		Press (Torr)	WFC (Volts)		
Ethylene	20°	1×10^{-8}	- 1.5	diffuse (1/2 0) features	1×10^{-8}	- 1.2	(1×1)	$(\sqrt{2}\times\sqrt{2})R45°$
	250°	1×10^{-8}	- 1.7	disordered	1×10^{-8}	- 1.5	(1×1)	disordered
Graphitic Overlayer	950°		- 1.1	ringlike diffraction features		- 1.0	(1×1)	ringlike diffraction features
n-Hexane	20°	5×10^{-8}	- 1.1	disordered	5×10^{-8}	- .8	(1×1)	disordered
	20°	5×10^{-8} (5 hrs)	- .9	disordered	5×10^{-8} (5 hrs)	- .6	(1×1)	disordered
	250°	5×10^{-8}	- 1.5	disordered	5×10^{-8}	- 1.2	(1×1)	disordered
Isoquinoline	20°	6×10^{-8}	- 1.9	diffuse (1/3 0) and (2/3 0) features	6×10^{-8}	- 2.1	(1×1)	disordered
Mesitylene	20°	4×10^{-8}	- 1.7	Streaks at 1/3.4 order diffuse (2/3.4 0) features	4×10^{-8}	- 1.7	(5×1)	1/3 order streaks
	20°	4×10^{-7}	- 1.35	disordered	4×10^{-7}	- 1.2	(1×1)	disordered
2-Methyl-naphthalene	20°	6×10^{-8}	- 2.0	very poorly ordered	4×10^{-9}	- 1.6	faint (5×1)	disordered
Naphthalene	20°	9×10^{-9}	- 1.95	apparent (3×1)	9×10^{-9}	- 1.7	(1×1)	disordered
	150°	9×10^{-9}	- 2.0	(6×6)	9×10^{-9}	- 1.65	(1×1)	disordered
Nitrobenzene	20°	9×10^{-9}	- 1.5	diffuse (1/3 0) features (pattern electron beam sensitive)	9×10^{-9}	- 1.4	(1×1)	disordered
Piperidine	20°	8×10^{-8}	- 2.1	disordered	8×10^{-8}	- 2.05	faint (5×1)a	disordered
Propylene	20°	2×10^{-8}	- 1.3	(2×2) (pattern electron beam sensitive)	2×10^{-8}	- 1.2	(1×1)	1/2 order streaks (pattern electron beam sensitive)
Pyridine	20°	1×10^{-8}	- 2.7	diffuse (1/2 0) features	1×10^{-8}	- 2.4	(1×1)	disordered
	250°	1×10^{-8}	- 1.7	well defined streaks at 1/3, 2/3, 3/3 order	1×10^{-8}	-	(1×1)	$(\sqrt{2}\times\sqrt{2})R45°$
Pyrrole	20°	6×10^{-8}	- 1.45	diffuse (1/2 0) features (pattern electron beam sensitive)	6×10^{-8}	- 1.6	(1×1)	diffuse (1/2 0) features
Quinoline	20°	3×10^{-8}	- 1.45	diffuse 1/3 order streaks	3×10^{-8} (6 min)	-	(5×1)	diffuse 1/3 order streaks
					3×10^{-8} (14 min)	- 1.7	(1×1)	disordered
Styrene	20°	6×10^{-8}	- 1.7	streaks at 1/3 order	6×10^{-8}	- 1.65	(1×1)	very poorly ordered
Toluene	20°	1×10^{-9}	- 1.7	streaks at 1/3 order	1×10^{-9}	- 1.55	(5×1)	streaks at 1/3 order
	150°	1×10^{-9}	- 1.65	(4×2)	1×10^{-9}	- 1.5	(1×1)	disordered
m-Xylene	20°	1×10^{-8}	- 1.8	streaks at 1/2.6 order	1×10^{-8}	- 1.65	(5×1)	streaks at 1/3 order

Figure Captions

Fig. 1 Scheme of the low-energy electron diffraction technique.

Fig. 2 Diffraction pattern of the (111) face of a platinum single crystal at four different incident electron beam energies: (a) 51 eV; (b) 63.5 eV; (c) 160 eV; (d) 181 eV.

Fig. 3 Translation vectors $\underset{\sim}{a}$, $\underset{\sim}{b}$ for the hexagonal Bravais lattice and corresponding reciprocal lattice vectors $\underset{\sim}{a}^*$, $\underset{\sim}{b}^*$. Note that the reciprocal lattice is a hexagonal lattice rotated by 30° with respect to the crystal lattice.

Fig. 4 Schematic of the c(2 x 2) adsorbate structure on a square lattice substrate illustrating the primitive ($\sqrt{2}$ x $\sqrt{2}$) - R45° adsorbate unit cell(solid lines) and the centered (2 x 2) adsorbate unit cell(dashed lines) in terms of the substrate unit cell vectors $\underset{\sim}{a}$, $\underset{\sim}{b}$. The adsorbate atoms (small heavy circles) are shown in four-fold coordinated bonding sites above substrate atoms (large open circles).

Fig. 5 Comparisons between theory and experiment of low-energy electron diffraction intensity-energy spectra for the (00) beam, Ni(001) at room temperature and for three incident beam angles. The theoretical calculations are from Tong and Kesmodel (Ref. 20) using a five phase-shift, five-layer multiple-scattering computer program. The experimental results are from Demuth and Rhodin (Refs. 98-99).

Fig. 6 Diffraction pattern of the Pt(100)-(5 x 1) structure at 124 eV.

Fig. 7 Directions of cuts in the crystallographic zones for the stepped, high Miller index surfaces listed in Table I.

Fig. 8 Diffraction patterns and schematic representations of stepped platinum surfaces.

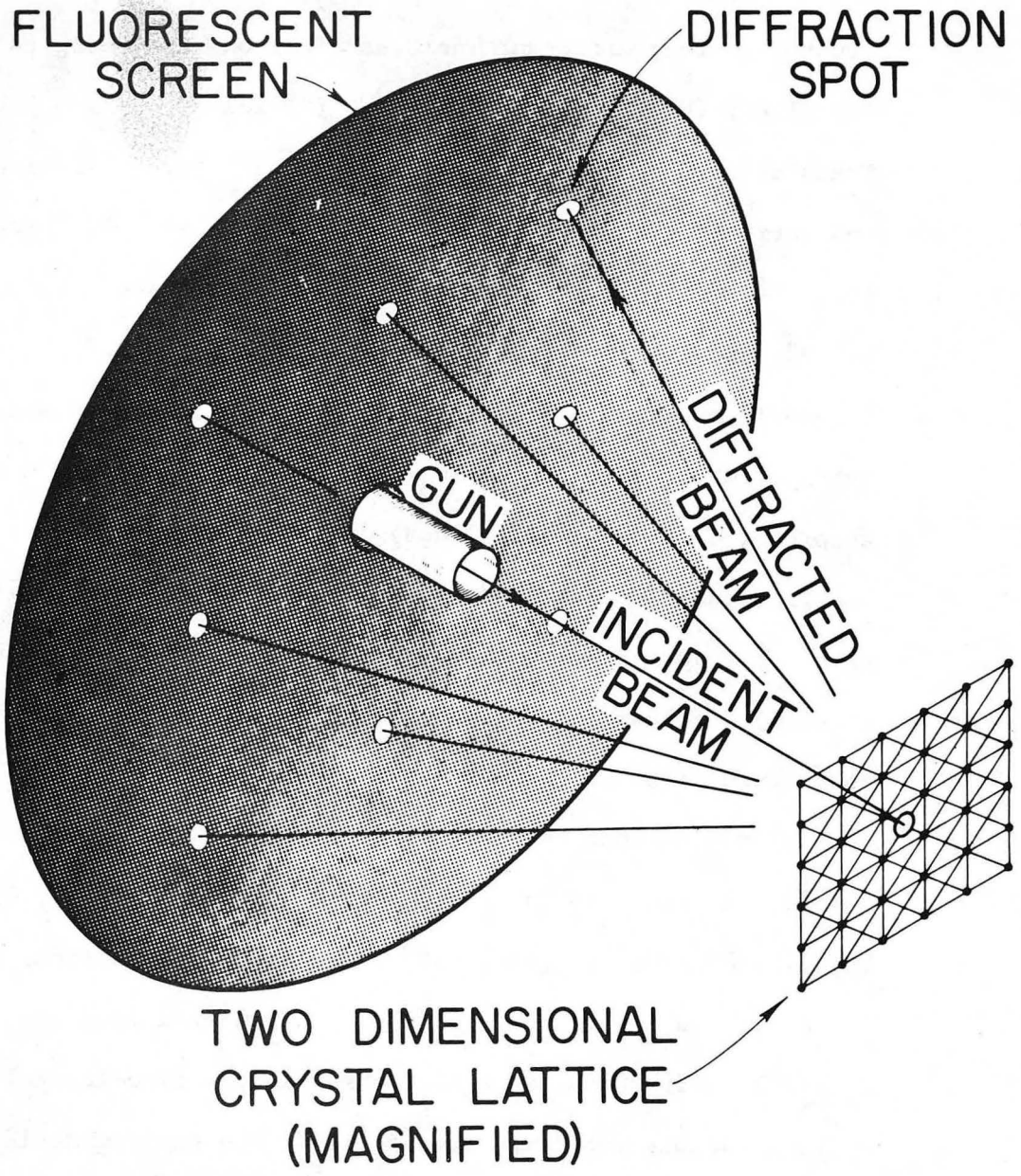

XBB708-3583

Fig. 1

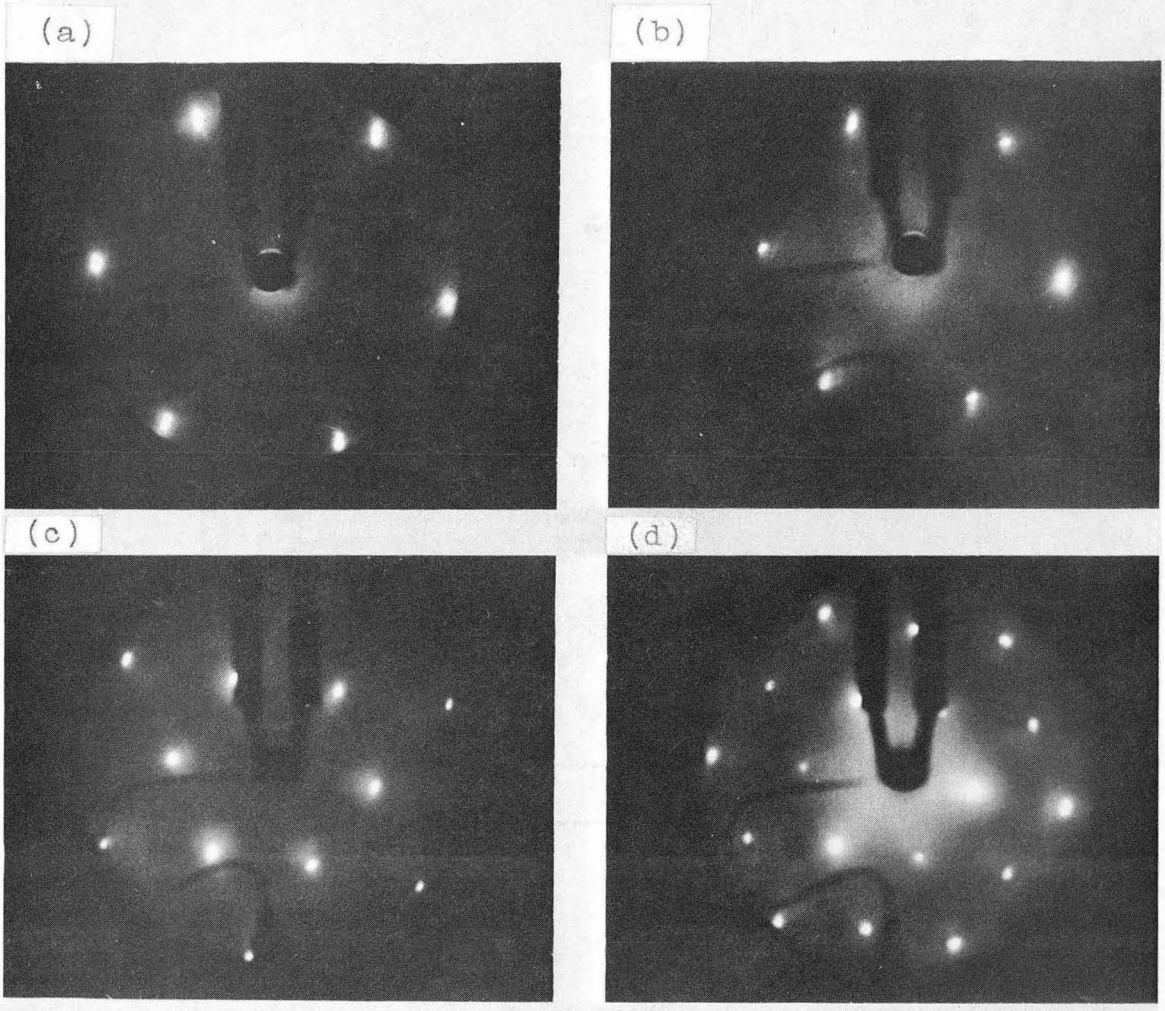

XBB708-5685

Fig. 2

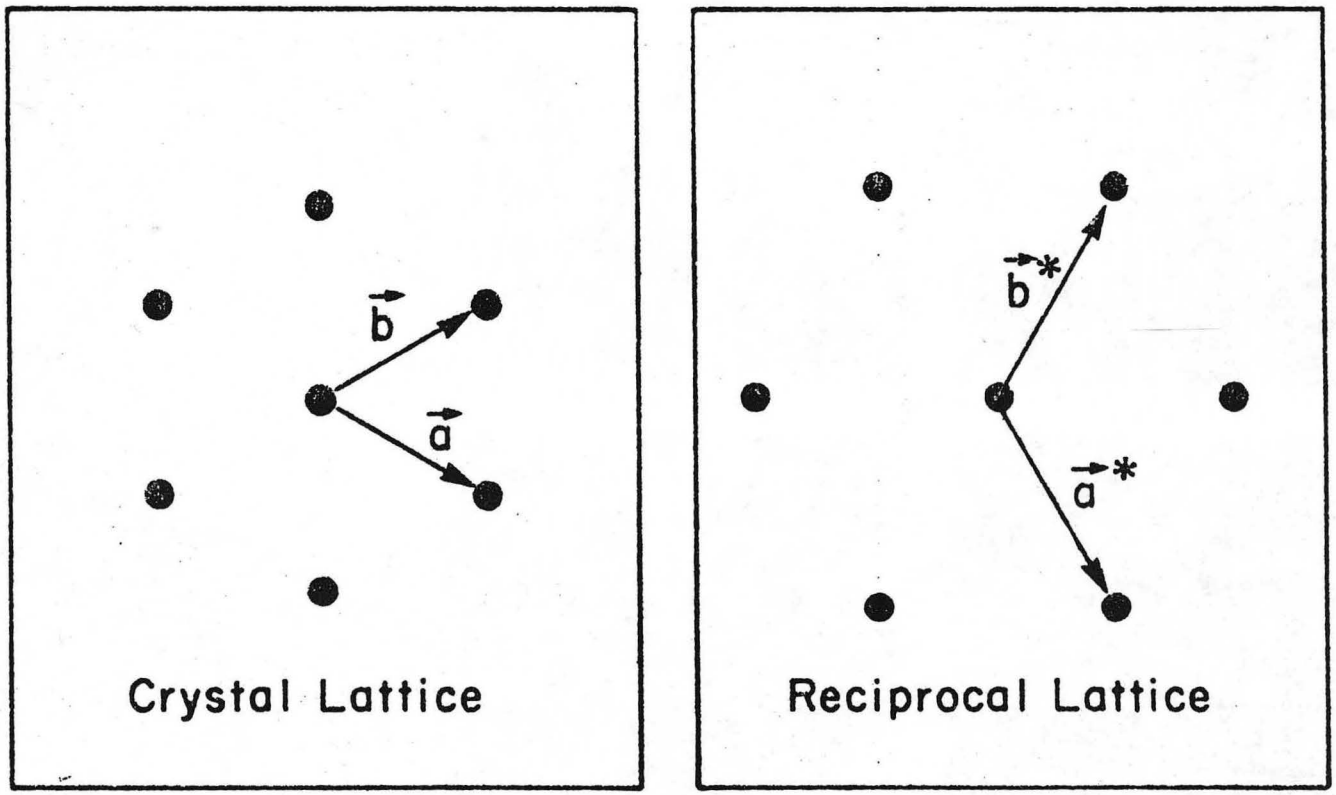

XBL 748-7095

Fig. 3

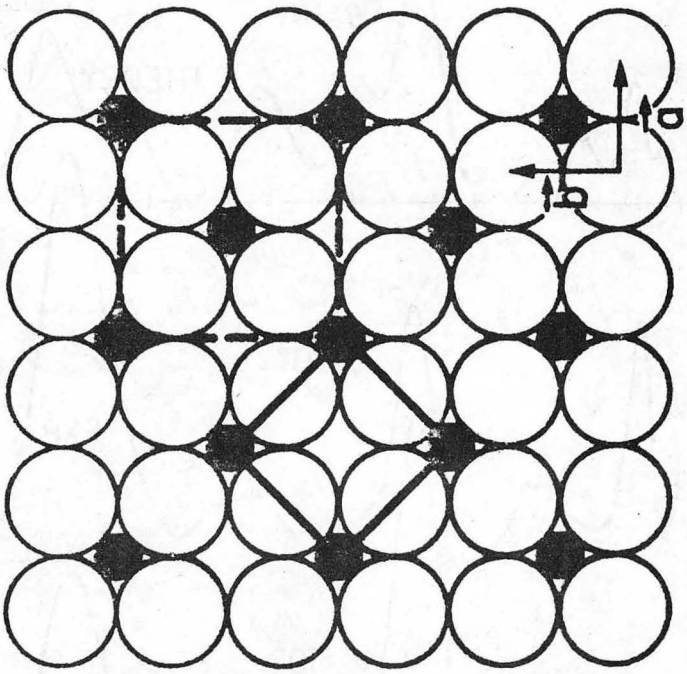

XBL 748-7096

Fig. 4

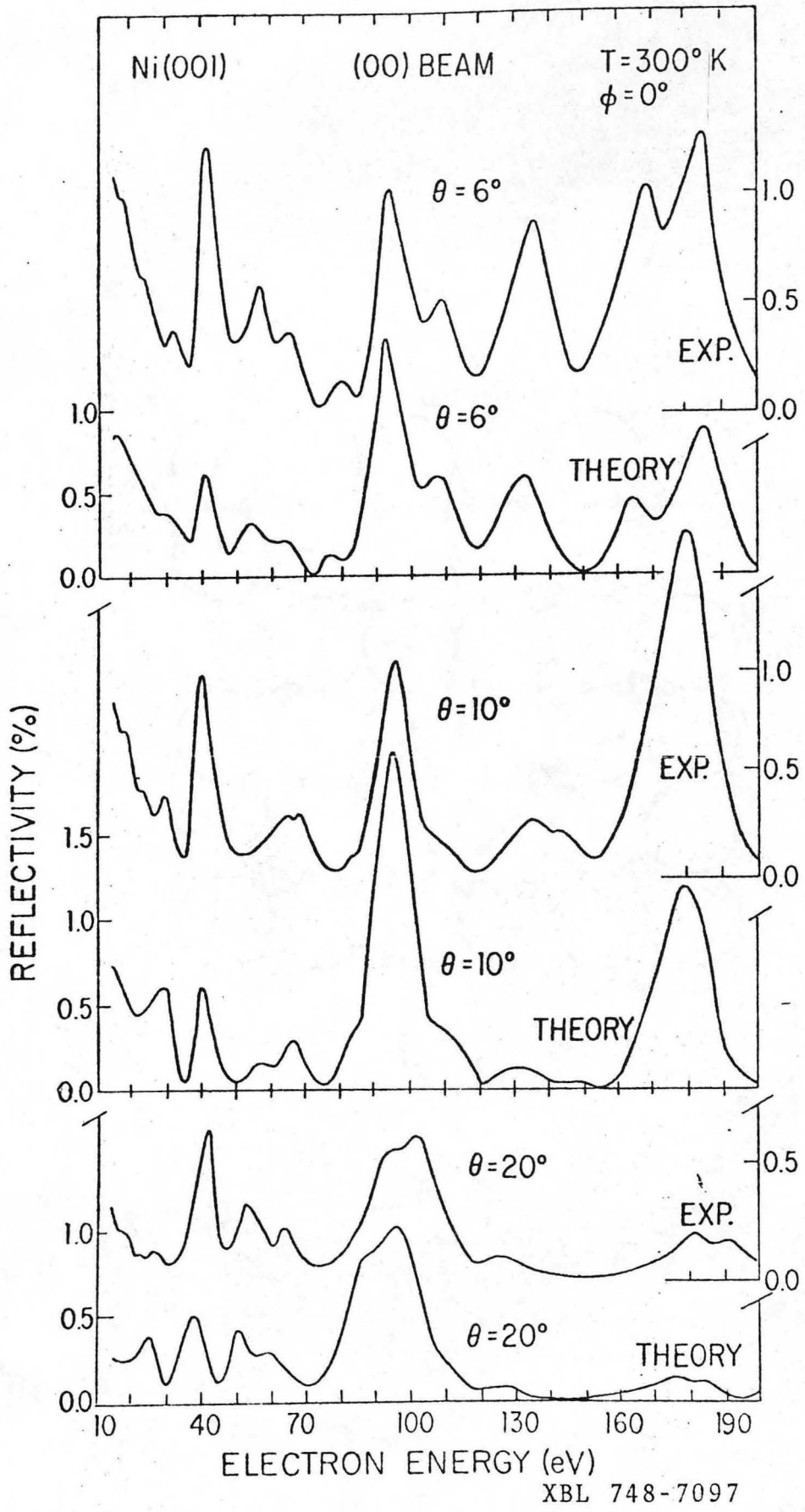
Ni(001)
(00) BEAM
T=300° K
ϕ=0°
θ=6°
EXP.
θ=6°
THEORY
θ=10°
EXP.
θ=10°
THEORY
θ=20°
EXP.
θ=20°
THEORY
REFLECTIVITY (%)
ELECTRON ENERGY (eV)
10
40
70
100
130
160
190
XBL 748-7097

Fig. 5

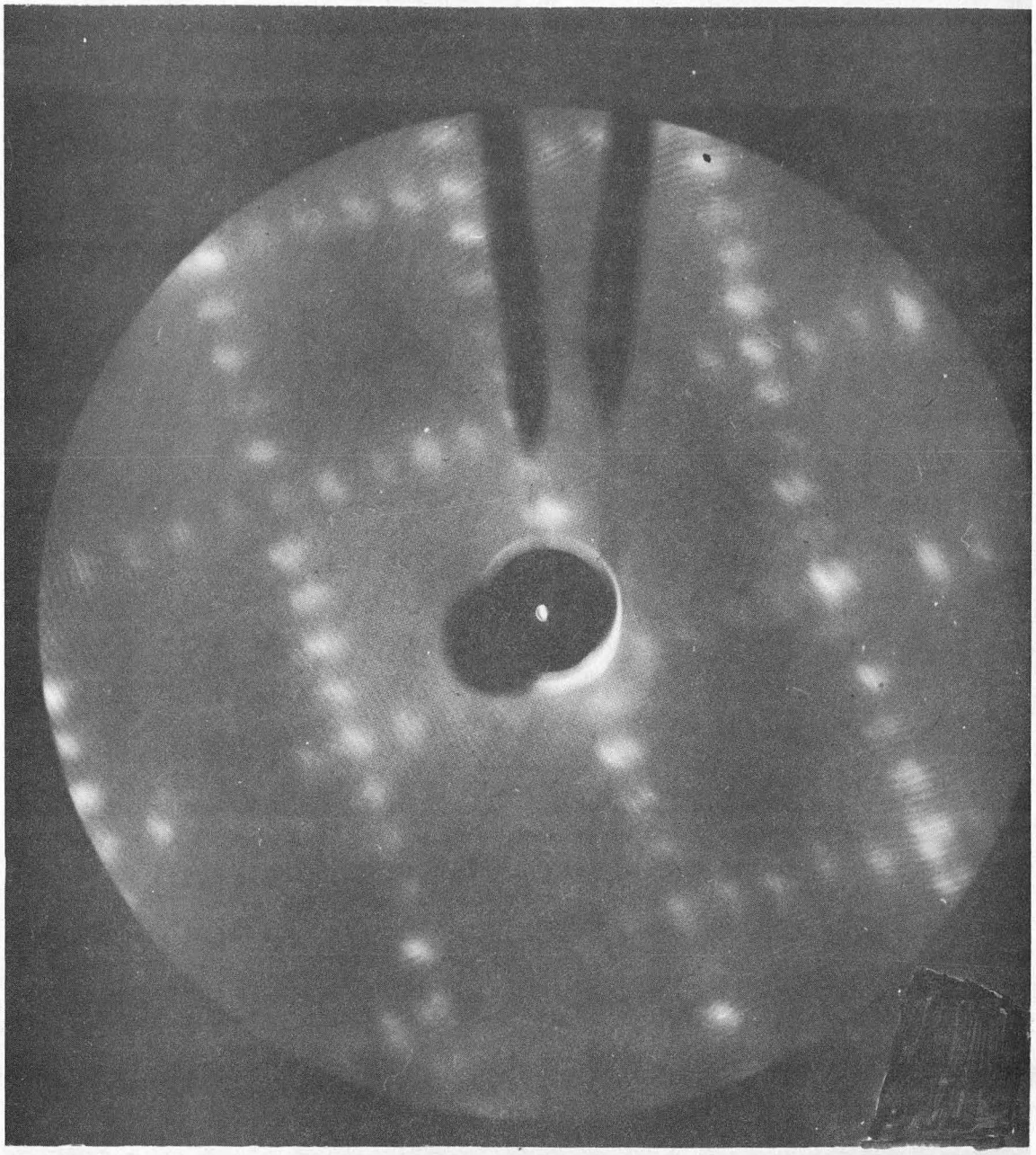

XBB708-3582

Fig. 6

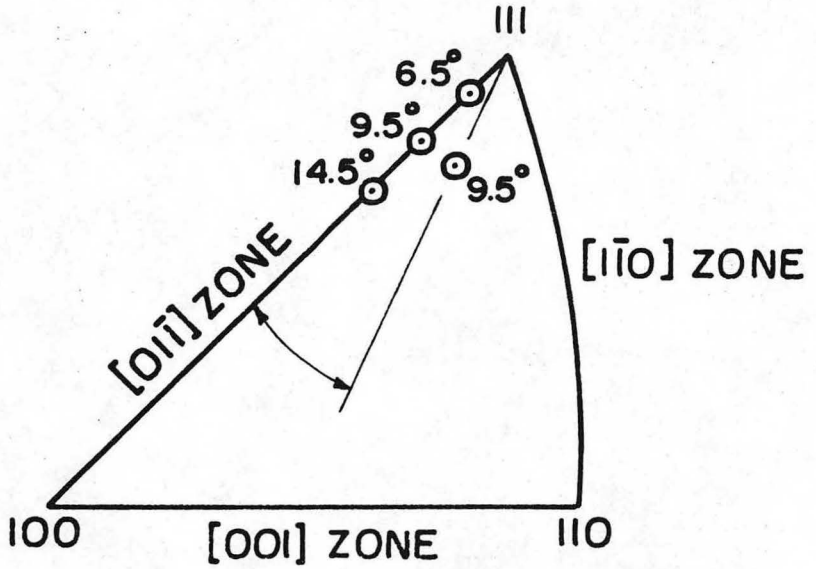

XBL 733-5906

Fig. 7

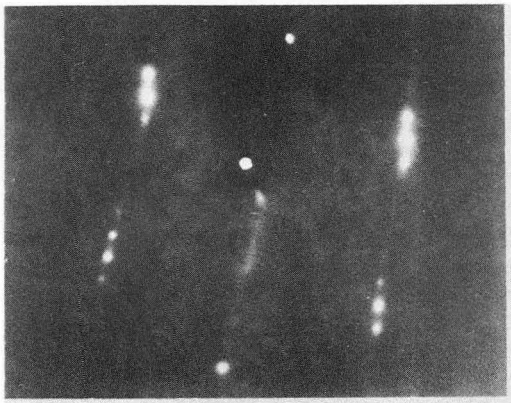

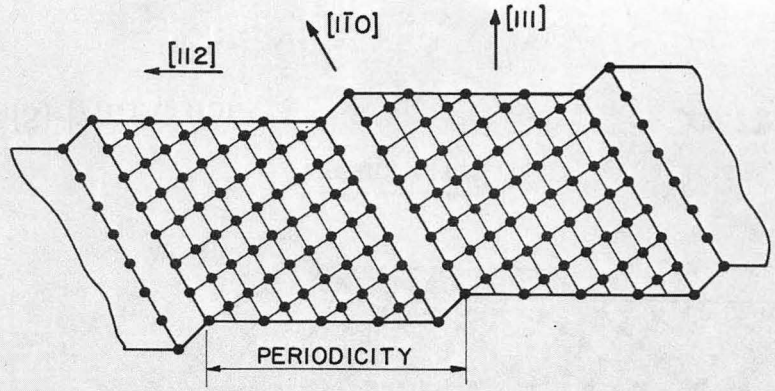

A. $P_T(S)$-[9(111)x(100)]

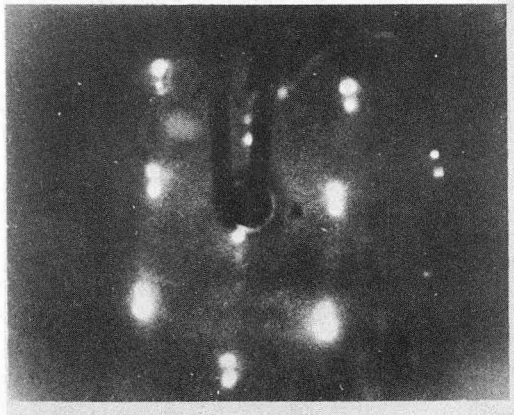

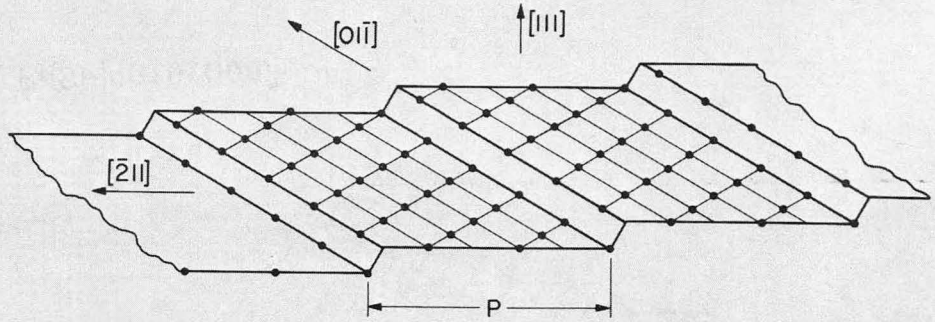

XBB735-2960

B. $P_T(S)$-[6(111)x(100)]

Fig. 8

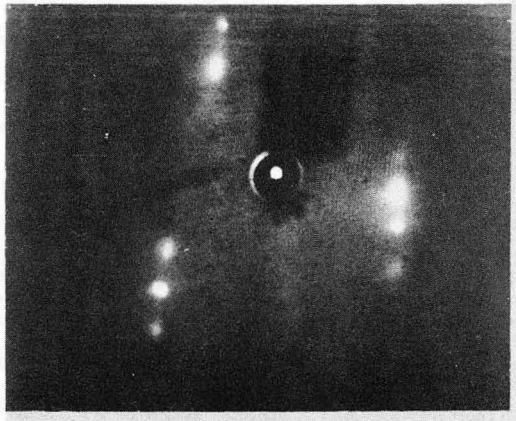

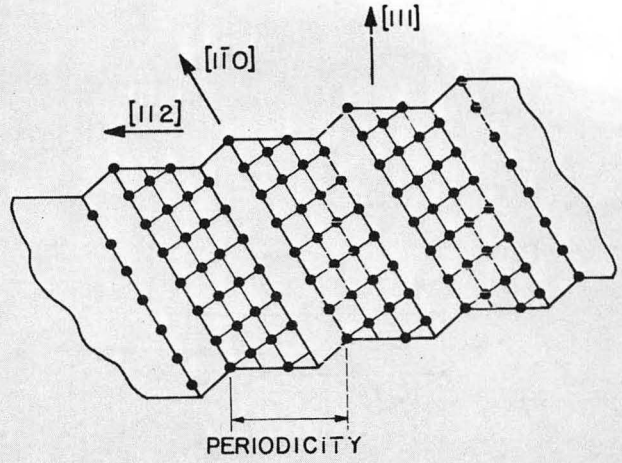

C. $P_T(S)$-[4(111)x(100)]

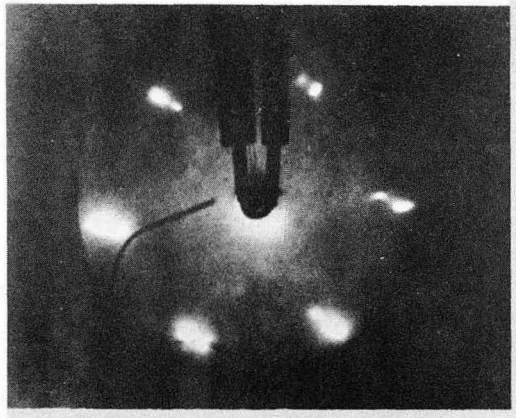

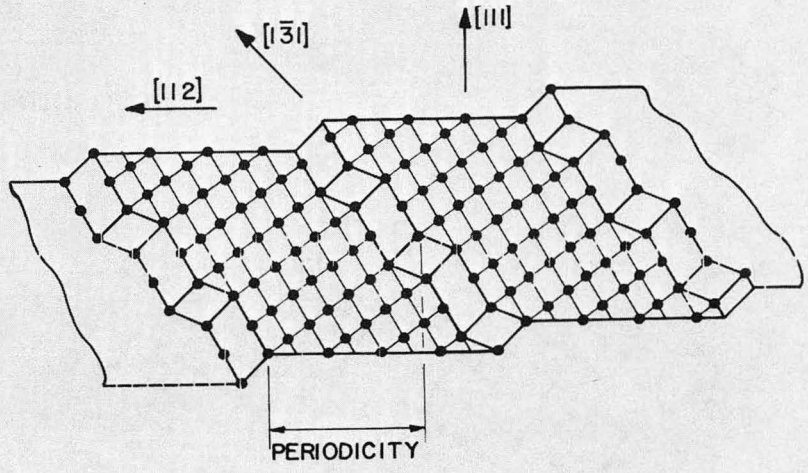

D. $P_T(S)$-[7(111)x(310)]

XBB735-2961

Fig. 8

TECHNICAL INFORMATION DIVISION
LAWRENCE BERKELEY LABORATORY
UNIVERSITY OF CALIFORNIA
BERKELEY, CALIFORNIA 94720